Reactive Transport Modeling for Exploring the Potential of Water Quality Sensors to Estimate Hydrocarbon Levels in Groundwater

Wu, C. L. R.; Wagterveld, R. M.; van Breukelen, B. M.

DOI
10.1029/2023WR036644

Publication date
2024

Document Version
Final published version

Published in
Water Resources Research

Citation (APA)
Wu, C. L. R., Wagterveld, R. M., & van Breukelen, B. M. (2024). Reactive Transport Modeling for Exploring the Potential of Water Quality Sensors to Estimate Hydrocarbon Levels in Groundwater. *Water Resources Research*, *60*(4), Article e2023WR036644. https://doi.org/10.1029/2023WR036644

AGU ADVANCING EARTH AND SPACE SCIENCES

Water Resources Research

RESEARCH ARTICLE
10.1029/2023WR036644

Reactive Transport Modeling for Exploring the Potential of Water Quality Sensors to Estimate Hydrocarbon Levels in Groundwater

C. L. R. Wu[1,2], **R. M. Wagterveld**[2], **and B. M. van Breukelen**[1]

[1]Department of Water Management, Faculty of Civil Engineering and Geosciences, Delft University of Technology, Delft, The Netherlands, [2]Wetsus, European Centre of Excellence for Sustainable Water Technology, Leeuwarden, The Netherlands

Key Points:

- In-situ water quality sensors are highly correlated with petroleum hydrocarbons in groundwater when spatiotemporal variability is considered
- DO and ORP are important for early detection, while pH and EC for long-term prediction of hydrocarbon contamination in groundwater
- The aquifer's hydrogeology impacts hydrocarbon-water quality correlations by influencing buffering capacity and flow velocity, among others

Supporting Information:

Supporting Information may be found in the online version of this article.

Correspondence to:

C. L. R. Wu,
c.l.wu@tudelft.nl

Citation:

Wu, C. L. R., Wagterveld, R. M., & van Breukelen, B. M. (2024). Reactive transport modeling for exploring the potential of water quality sensors to estimate hydrocarbon levels in groundwater. *Water Resources Research*, *60*, e2023WR036644. https://doi.org/10.1029/2023WR036644

Received 3 NOV 2023
Accepted 1 MAR 2024

Author Contributions:

Conceptualization: R. M. Wagterveld, B. M. van Breukelen
Data curation: C. L. R. Wu
Formal analysis: C. L. R. Wu
Funding acquisition: R. M. Wagterveld, B. M. van Breukelen
Investigation: C. L. R. Wu
Methodology: C. L. R. Wu
Project administration: R. M. Wagterveld, B. M. van Breukelen
Resources: C. L. R. Wu
Supervision: R. M. Wagterveld, B. M. van Breukelen
Validation: C. L. R. Wu

Abstract Petroleum products have contaminated groundwater with harmful organic compounds, such as benzene, toluene, ethylbenzene, and xylenes (BTEX). Collecting and analyzing polluted groundwater samples is expensive and undertaken infrequently. However, quick remedial action in case of unexpected events requires continuous monitoring. In-situ water quality sensors (pH, EC, DO, ORP) may show correlations with the components of dissolved petroleum hydrocarbon (PHC) such as aromatics and non-volatile mobile fractions. Correlations are prerequisite to ultimately develop real-time prediction models. Since suitable field data sets are limited, we simulated the fate of hydrocarbons in groundwater under various realistic conditions using a reactive transport model as novel approach to explore when, where, and why correlations occur. A stationary oil source zone continuously dissolved at the top of a heterogeneous and shallow sandy aquifer over a two-dimensional cross-section. Our model considered transient conditions (fluctuating water table) and spatially uniform hydrogeochemical composition. We observed a strong correlation between PHCs and water quality sensors (rolling Spearman's correlation > |0.8|) at varying periods. These correlations are strongly affected by the location of observation wells, the aquifer's hydraulic conductivity, and the availability of calcite and oxide minerals, and other electron acceptors. DO and ORP are significant for the early detection of hydrocarbon contamination, whereas pH and EC are important features for the long-term monitoring of hydrocarbons. Our findings lay the foundation for the subsequent development of a data analysis model to detect and estimate in real time PHC levels in groundwater using in-situ water quality sensors.

Plain Language Summary Groundwater contamination by petroleum products, including benzene, toluene, ethylbenzene, and xylenes (BTEX), is a serious environmental concern. However, the collection and analysis of polluted groundwater samples are expensive and infrequently conducted. In the event of unexpected contamination, quick remedial action is crucial, which requires continuous monitoring of groundwater quality. We investigated whether in-situ water quality sensors like pH, electrical conductivity (EC), dissolved oxygen (DO), and oxidation-reduction potential (ORP) can predict the concentration of dissolved petroleum hydrocarbons (PHC) in groundwater. Understanding the correlations between these sensors and PHC levels is essential for developing real-time prediction models. Since field data is scarce, we developed a reactive transport model that simulates the movement of PHC in groundwater under different conditions. Our model simulated a scenario where oil continuously dissolves at the top of a sandy aquifer. The correlation between PHC levels and water quality sensors varies depending on the location and timing of measurements. DO and ORP are particularly useful for detecting early signs of contamination, while pH and EC are important for long-term monitoring. Our findings provide the foundation for developing data analysis models capable of real-time detection and estimation of PHC levels in groundwater using water quality sensors.

1. Introduction

The widespread use of petroleum products has caused groundwater contamination with dissolved petroleum hydrocarbons (PHC). These compounds are detrimental to both human health and the environment, especially the benzene, toluene, ethylbenzene, and xylenes (BTEX) (Li et al., 2021; Ololade et al., 2021). Leakages from underground storage tanks (Hadley et al., 2015) or burst buried oil pipes release hydrocarbons that tend to migrate toward the water table and further into the groundwater (Peter, 2010; Teramoto & Chang, 2019). Several processes are then triggered by the generated groundwater pollution plume, including degradation. These processes have been found to change the groundwater composition. Although the contamination of drinking water by PHC

Visualization: C. L. R. Wu
Writing – original draft: C. L. R. Wu
Writing – review & editing: R. M. Wagterveld, B. M. van Breukelen

poses a threat to public health, groundwater is only monitored for possible pollutants from one to six times per year (Ayscough et al., 2002; Ross, 2013). This may lead to the late detection of any contamination, a delayed response time after a leakage, and an increased cost in remedial actions.

The European Union has identified millions of leaking storage tanks (European Commission, 2001). The current practice of manually collecting groundwater samples is expensive and has associated health risks (US EPA, 2003; Wu et al., 2017; Zanello et al., 2021). As a result, we need a reliable, low maintenance, and low-cost technology that enables the early detection and real-time monitoring of contaminants in groundwater. Various efforts have been made to develop this kind of technology. Some studies applied sensors to estimate the level of hydrocarbons directly and rapidly in groundwater (Bender et al., 2012; Buerck et al., 2001; Erickson & Lear, 2014; US EPA, 2003). Still, these sensors are expensive, demand high maintenance, and require large construction projects.

In general, the challenges associated with PHC monitoring in groundwater originate from low-resolution data from manual sampling, and the high cost and maintenance of existing PHC sensors. Virtual sensors are among the recent technological solutions used to address these challenges. In principle, virtual sensors are developed by combining the signals received from physical sensors typically through sensor data fusion. These signals are embedded into complex functions or analytics algorithms to measure variables or conditions that might not be easily measurable physically (Kabadayi et al., 2006; Martin et al., 2021). Virtual sensors were recently applied to estimate uranium and tritium in groundwater over time using specific conductance and pH sensors (Schmidt et al., 2018). This real-time monitoring system was able to observe the evolution of the radionuclide plume. However, no attempts have yet been made to use virtual sensors to detect and estimate PHC concentration in groundwater.

The development of a virtual sensor involves identifying the relevant parameters and establishing their relationships. These parameters are then combined, typically by using analytics algorithms, to measure the variable of concern (Martin et al., 2021). The current paper is solely focused on the initial stage of virtual sensor development. The goal of this paper, therefore, is to explore the potential of water quality sensors, such as pH, dissolved oxygen (DO), redox level (ORP), and electrical conductivity (EC), to predict and monitor the level of PHC in groundwater.

Since the available data on groundwater contaminated sites are insufficient for a robust statistical analysis, a reactive transport model (RTM) to simulate the fate and transport of PHC compounds in the aquifer can be developed as data source. RTMs have shown that hydrocarbons in groundwater can trigger geochemical and biological reactions. Previous RTM studies have simulated the migration of PHC plumes in groundwater by combining the effects of advection, mechanical dispersion, and molecular diffusion (Cavelan et al., 2022; Picone, 2012), equilibrium and kinetic dissolution of PHC compounds (Lekmine et al., 2014; Molson & Eng, 2011), aerobic and anaerobic PHC biodegradation (Colombani et al., 2009; Miles et al., 2008; Ng et al., 2015; Prommer et al., 2002; Schreiber et al., 2004; Vencelides et al., 2007), dissolution and precipitation of carbonate minerals (Maurer & Rittmann, 2004; Spence et al., 2005), sorption of dissolved PHC to organic matter in sediments (Gharedaghloo & Price, 2021; Valsala & Govindarajan, 2018), and (de)sorption of mobilized ions (Cozzarelli et al., 2016; Miles et al., 2008; Ziegler et al., 2017).

These processes have been found to change the physical and chemical properties of the aquifer including pH, DO, and ORP (Appelo & Postma, 2005; Ng et al., 2014). Thus, the RTM can provide mechanistic insights into the parameter correlations and help elucidate the effect of site-specific factors on these correlations. Furthermore, the RTM has no limitations on virtual data sets that can be produced.

We therefore developed a generic RTM that simulated under presentative conditions the fate and transport of hydrocarbons in groundwater and associated biogeochemical processes. Then we quantified the correlation between in-situ water quality parameters (iWQP) and PHC concentration, specifically BEX and the non-volatile dissolved organic carbon, NVDOC). Finally, we assessed the effect of different factors in terms of spatiotemporal, hydrogeological, and geochemical properties of the aquifer to the identified correlations.

2. Materials and Methods

We developed an RTM simulating groundwater flow and reactions under hypothetical but realistic aquifer conditions to provide temporal and spatial data sets needed for correlation analysis under various field conditions. The model domain and parameters were based on existing studies that examine PHC contamination. Our study

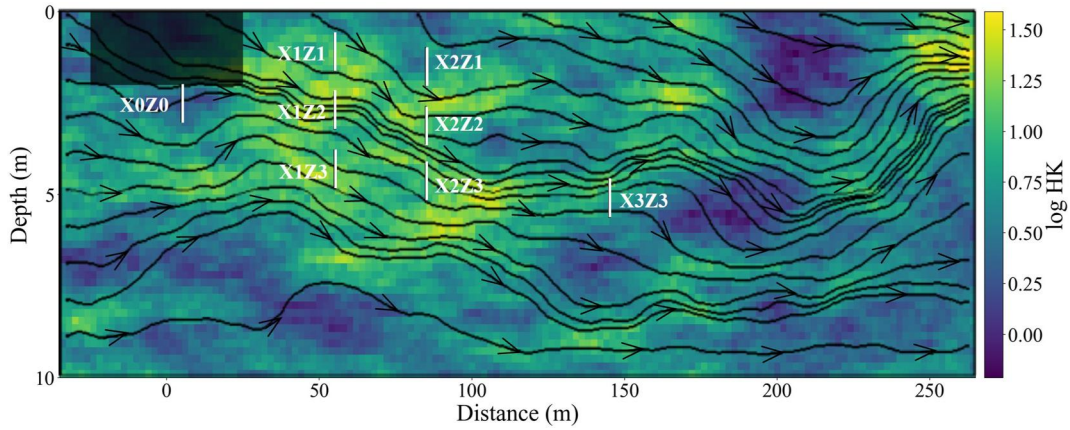

Figure 1. Logarithmic hydraulic conductivity field (log of m/day) and the steady-state flow paths with the oil body location (shaded area) and observation wells. Well names are based on the distance from the oil body (X1 nearest, X3 farthest), and the depth (Z1 shallowest, Z3 deepest). X0Z0 is located below the oil body.

was specifically inspired by existing studies on the crude oil spill site in Bemidji, Minnesota, which is one of the most studied oil contaminated sites in the world (Ng et al., 2015).

2.1. Base Model Development

Our reactive transport model was set-up in Jupyter notebook using FloPy, an open-source Python-based modeling tool for creating, running, and post-processing groundwater models (Bakker et al., 2016). We used MODFLOW 2005 (Harbaugh, 2005) to solve the groundwater flow equation utilizing a finite-difference numerical solution, and MT3DMS (Zheng et al., 2012) to simulate the contaminant transport in the aquifer by activating the advection and dispersion packages. We then used PHT3D (Prommer & Post, 2010) to manage the coupling of flow and transport with geochemical reactions from PHREEQC-2 (Parkhurst & Appelo, 2000). We included multicomponent dissolution of LNAPL (Molins et al., 2010; Ng et al., 2015), first-order aerobic and anaerobic biodegradation (Salanitro, 1993; D'Affonseca et al., 2011; Ng et al., 2015), mineral-phase reactions (Molins et al., 2010; Ng et al., 2015; Teramoto & Chang, 2019), cation exchange (Ng et al., 2015), and outgassing of methane, CO_2, and N_2 (Amos et al., 2005; Ng et al., 2015). We also considered in our model a fluctuating water table as a transient driver and a heterogeneous hydraulic conductivity field.

The synthetic aquifer represented a saturated porous media that is 260 m in length and 7 m in thickness, as used by Ng et al. (2015) to simulate the Bemidji aquifer. We considered an aerobic aquifer with 0.25 mmol/L of O_2, 0.36 mmol/L of NO_3, and 0.52 mmol/L of SO_4. The pH value is 7.7 and the background EC is 339 μS/cm representing a freshwater aquifer. To prevent any boundary effects on the simulations, we extended the computational grid to a total length of 300 m and a total thickness of 10 m. The model domain has a discretization of 150 grid cells in the horizontal (x) direction and 50 grid cells in the vertical (z) direction (grid size of 2 m by 0.2 m). This is comparable with the previous Bemidji model with a grid size of 4.3 m by 0.47 m (Ng et al., 2015). For this model, we used a mean homogeneous porosity value of 0.38 (Dillard et al., 1997) and a longitudinal and transverse dispersivity of 1 and 0.04 m, respectively (Ng et al., 2015). We chose 0.01 as the aquifer storage coefficient and 0.20 as the storage yield, both within the values for an unconfined aquifer (Lohman, 1972). Table S1 in Supporting Information S1 summarizes the parameters used for the flow and physical transport model.

2.2. Heterogeneous Hydraulic Conductivity

A heterogeneous sandy aquifer was represented using a heterogeneous hydraulic conductivity (HK) field (Figure 1) generated using the field generator package of PMWIN (Chiang & Kinzelbach, 2003). The HK field has a mean value of 6.2 m/d, resembling the findings (homogeneous value of 6.1 m/d) of an inverse modeling study which was previously conducted at the Bemidji site (Essaid et al., 2003). Using 0.3 as the common log standard deviation value, the minimum and maximum HK values were 0.53 and 51.74 m/day, respectively. This represents an aquifer consisting of fine and coarse sand according to the typical HK values of geological units (Domenico & Schwartz, 1998). Furthermore, we assumed a correlation length/field width along rows and

columns of 0.1. The PMWIN field generator is based on Mejia's algorithm and was used in different studies (Thouement & Van Breukelen, 2020; Zammouri & Ribeiro, 2017). Based on the commonly reported vertical-to-horizontal anisotropy ratio, we used 10% of the saturated HK as the vertical HK (e.g., 0.61 m/d for the mean HK value) (Todd, 1980).

2.3. Simulation of Transient Flow Conditions

Seasonally changing groundwater flow can affect the contaminant flow directions and plume spreading (Prommer et al., 2002). Although this was not considered in the previous modeling study conducted at Bemidji (Ng et al., 2015), we wanted to simulate the periodic changes in the water table. Generally, fluctuations could be caused by factors including seasonal variability in recharge, tidal actions, or dam operations, among others (Bakker & Post, 2022). Additionally, extreme events such as increased precipitation due to climate change can affect the water table by influencing groundwater recharge. Although previous studies have explored how climate change affects contaminant transport (Libera et al., 2019; Xu et al., 2022), our focus in this study did not extend to simulating the potential impacts of climate change.

To simulate the transient groundwater flow, we first established a steady-state flow field at the beginning. We simulated an average water table gradient of 0.0035 m/m for day 1, similar to the previous studies conducted at the Bemidji site (Essaid et al., 2003; Ng et al., 2015). This was achieved by imposing a constant head boundary condition at the left and right model boundaries, and a uniform recharge flux of 178 mm/year (Ng et al., 2015) at the upper layer of the model domain. We considered the model bottom as a no flow boundary, assuming that an impermeable clay layer is present.

We then simulated the transient groundwater flow by imposing a general head boundary (GHB) condition with a monthly changing head at the left model boundary (Anderson et al., 2015). The GHB condition represented a monthly water table fluctuation (WF) caused by open water in direct contact with the aquifer at the upstream part of the model. A commonly observed pattern in groundwater level variation is a cyclic water-level fluctuation (Healy & Cook, 2002; Jiang et al., 2017; Neto et al., 2016; Park & Parker, 2008). Thus, we used a simple sinusoidal function (Bakker, 2019; Wu et al., 2021) with an amplitude of 0.25 and a period of 12 months to approximate the monthly variations in groundwater level at the left boundary. This amplitude corresponds to the maximum observed change in water level (0.5 m) at the Bemidji site (Essaid et al., 2003). The WF at the right boundary, however, was based on a larger model with a length of 5,200 m. Detailed description of this larger model can be found in the Supporting Information (Text S1, Figure S1 in Supporting Information S1). In this larger model, we imposed a fluctuating water table on the left boundary and a constant head on the right boundary. We then recorded the water table response in an observation well 300 m from the left boundary and used it as the right boundary condition in the final model (Figure S2 in Supporting Information S1). Note that at the right boundary, the amplitude was dampened, and the peak arrived later.

Moreover, since the change in the water table was much smaller than the considered saturated thickness, we assumed a constant transmissivity for the unconfined synthetic aquifer (Bakker & Post, 2022). The total simulation time was 100 years, based on studies showing that contamination of petroleum hydrocarbons in aquifers can last for decades to over a century (Kulkarni et al., 2020; Pishgar et al., 2022). There were 1,201 stress periods with 30 days per stress period (monthly stress period for 100 years plus 1 day of steady state at the beginning to establish a steady state flow field). We used daily timesteps with sufficiently small grid cells to prevent any convergence issues caused by numerical oscillations and dispersions.

2.4. Initial Hydrogeochemical Conditions

For the initial background concentration of ions and physical properties of the aquifer, we adopted the values from the Bemidji site studies (Bennet et al., 1993; Ng et al., 2015). The model does not include the Mn element for simplification since we assumed Mn to behave similarly to Fe because of similar geochemical properties in aquatic environments (Rusydi et al., 2021). The recharge composition was similar with the native groundwater. Using PHREEQC, we first charge balanced and equilibrated the background concentrations with calcite, resulting in the parameter values shown in Table S2 in Supporting Information S1.

We included 131.6 mmol/kg dissolvable calcite in the model because of its contribution to the aquifer's pH-buffering and carbonate chemistry, and set the saturation index to 0.05 (Ng et al., 2015). We also included

7.6 mmol/kg of the mineral phase electron acceptor amorphous ferric hydroxide ($Fe(OH)_3$) that exists at the Bemidji site (Ng et al., 2015). The electron donor siderite ($FeCO_3$) was configured to precipitate in response to increasing dissolved ferrous iron levels because of iron-oxide reduction. Pyrite was also included in our model but not in Ng et al. (2015) because the presence of sulfate was not found at the Bemidji site. Pyrite was allowed to precipitate as a sink for Fe^{2+} and H_2S. Table S3 in Supporting Information S1 lists the minerals included in the model, along with the Log K values.

2.5. Fate and Transport Component

2.5.1. Simulation of NAPL Dissolution

The contamination of the aquifer by PHCs starts with the dissolution of the light non-aqueous phase liquid (LNAPL), referred to in this study as the source zone. Dimension of the source zone varies at different sites, ranging from less than 5 m in length and less than 1 m in thickness (Freitas et al., 2011; Gomez & Alvarez, 2010; Prommer et al., 2009; Xu et al., 2015) to more than 50 m in length (D'Affonseca et al., Miles et al., 2008) and more than 1 m in thickness (Ng et al., 2015; Suarez & Rifai, 2004). In this study, we assumed the dimensions of the oil body to be 50 m in length and 2 m in thickness situated at the uppermost layer and 10 m downstream from the left boundary. The location of the left boundary, x is −35 m with reference to the center of the source zone (Figure 1). Following the Bemidji studies (Essaid et al., 2003; Ng et al., 2015), we ignored the slow movement of the oil phase and assumed the source zone to be stationary for modeling simplification (Dillard et al., 1997).

Oil saturation can vary depending on factors such as the spill size, the NAPL composition and thickness, and the aquifer characteristics (Lenhard et al., 2004, 2018; Mao et al., 2020). Previous reports have shown that LNAPL saturations may range from about 2% to 60% of the pore volume (Beckett & Lundegard, 1997; Huntley et al., 1994). We thus assumed a homogeneous oil saturation of 15%, comparable to the oil saturation values at the Bemidji area (Ng et al., 2014, 2015).

At the beginning of simulations, the LNAPL was partitioned into 4.3% BEX (C_6H_6) for combined benzene, ethylbenzene, and xylene; 1.3% toluene (C_7H_8); 39.2% preNVDOC ($C_{19}H_{24}O_6$) for "oil phase precursors to non-volatile dissolved organic carbon (NVDOC)" (Thorn & Aiken, 1998); 16.1% long-chain n-alkanes ($C_{15}H_{32}$); and 16% short-chain n-alkanes ($C_{11}H_{25}$). The remaining oil pool (23.1%), which does not dissolve nor degrade from the LNAPL, was considered unreactive (Baedecker et al., 2011; Ng et al., 2015). The partitioning and representative stoichiometries in the parentheses were adopted from Ng et al. (2015). These include short-chain n-alkane compounds representing all C_6-C_{12} n-alkanes, and long-chain n-alkane compounds representing all C_{13}-C_{32} n-alkanes. BEX compounds were grouped based on their similarities in migration and degradation (for more details, see Ng et al., 2014, 2015).

We also adopted from previous modeling studies the multicomponent solubility of organic carbons following Raoult's law (Essaid et al., 2003; Ng et al., 2015). This includes the simplification that toluene does not dissolve in groundwater but degrades directly from the source zone. The multicomponent dissolution kinetics from a stationary oil body adequately represented the observations at the Bemidji site (Essaid et al., 2003; Ng et al., 2015).

2.5.2. Hydrocarbon Degradation

We simulated the aerobic and anaerobic biodegradation of PHCs using the partial equilibrium approach (Jakobsen & Postma, 1999). This was derived from the modeling study previously conducted at the Bemidji site (Ng et al., 2015). In general, this approach assumes that the kinetically controlled oxidation of natural organic carbon (CH_2O):

$$CH_2O + 2\,H_2O \rightarrow HCO_3^- + 5\,H^+ + 4\,e^-, \quad (1)$$

is the rate-limiting step, while the reduction of the various terminal electron acceptors:

$$O_2 + 4\,H^+ + 4\,e^- \rightleftharpoons 2\,H_2O, \quad (2)$$

$$2\,NO_3^- + 12\,H^+ + 10\,e^- + \rightleftharpoons N_2 + 6\,H_2O, \quad (3)$$

$$Fe(OH)_3 + 3\,H^+ + e^- \leftrightharpoons Fe^{2+} + 3\,H_2O, \quad (4)$$

$$SO_4^{2-} + 9\,H^+ + 8\,e^- \leftrightharpoons HS^- + 4\,H_2O, \quad (5)$$

$$HCO_3^- + 9\,H^+ + 8\,e^- \leftrightharpoons CH_4 + 3\,H_2O, \quad (6)$$

is in equilibrium, thus governed by the Gibbs free energy. We also used the first-order biodegradation kinetics used by Ng et al. (2015), which was temporally and spatially uniform within the aquifer, and does not depend on the redox condition (Essaid et al., 2003). Although more complex biodegradation kinetics were previously used, such as varying degradation rate constants depending on redox conditions (Höyng et al., 2015) and Monod kinetics (Aronson et al., 1999; Essaid et al., 1995; Schreiber & Bahr, 2002), the first-order degradation model was found to be adequate for simulating the field conditions at the Bemidji site (Ng et al., 2015). We implemented individual degradation parameters for separate compounds that comprised the oil mixture, as a previous simulation study considered this essential (D'Affonseca et al., 2011). Ng et al. (2014, 2015) provide more details on the organic carbon degradation pathways and the rate constants used.

2.5.3. Cation Exchange and Sorption

Like the previous model at the Bemidji site (Ng et al., 2015), we simulated basic cation exchange. However, instead of including only Fe^{2+}, Mn^{2+}, and H^+ in ion exchange, we also considered the four major cations Ca^{2+}, Mg^{2+}, K^+, Na^+ (Appelo & Postma, 2005), aside from Fe^{2+}, as exchangeable cations to simulate a more generic aquifer. This is also in line with other RTM studies (van Breukelen et al., 2004). Based on Ng et al. (2015), we also assumed a cation exchange capacity (CEC) of 10.94 mol/kg for the aquifer. Then, we computed the distribution of exchangeable cations by equilibrating the cation exchanger with the initial groundwater composition using PHREEQC-2. Assuming that the fraction of organic carbon in the aquifer is low, we neglected the retardation of PHCs due to sorption on sedimentary organic matter.

2.5.4. Degassing From Solution

We simulated the degassing of CO_2, CH_4, and N_2 in this model to represent the carbon loss through outgassing. Following the implementation of Ng et al. (2015), outgassing was simulated in two parts: direct outgassing of CO_2 and CH_4 from the source zone, mainly from poorly soluble short and long-chain n-alkanes, and outgassing of gas species from aqueous solution, including the ones produced from biodegradation of BEX, toluene, and NVDOC, once the sum of partial pressures of CO_2, CH_4, and N_2 reaches the average hydrostatic pressure (Amos et al., 2005; Van Breukelen et al., 2004). We applied a depth gradient pressure threshold corresponding to the annual average hydrostatic pressure for each depth in the aquifer. For simplicity, the pressure increased from 1 atm at the water table to about 1.97 atm at 10 m depth, disregarding the effect of WF. Each gas species was allowed to outgas at a rate proportional to the fraction of partial pressure to the total pressure. A detailed description of the outgassing mechanism can be found in Amos et al. (2005), and Ng et al. (2015). Further details on the database used for the fate and transport equations can be found in the Supporting Information (Database S1 and S2 in Supporting Information S1), including the coefficients used, and the equilibrium and kinetic reactions with corresponding constants considered in the simulation.

2.6. Scenario Simulations

Contaminated sites have unique hydrogeologic conditions, hydraulic properties, and geochemical characteristics. We therefore simulated various scenarios to test the effect of aquifer conditions on the correlation between the concentration of PHCs and the iWQPs. First, we changed the amplitude of the WF in the general head boundary condition from 0.25 to 0.50 (WF+) and 0.75 (WF++) to consider the effects of this transient driver. Then, we changed the mean HK from 6.2 to 3.1 m/day (HK-) and 9.3 m/day (HK+) to consider the uncertainties in aquifer heterogeneities. We used the same heterogeneous field and dividing (multiplying) the values to decrease (increase) the mean HK. This kept the hydraulic conductivity values to still be within the reported range of HK for fine and medium sand (Domenico & Schwartz, 1998). We also varied the initial background concentration of ions from fresh groundwater (EC of 339 μS/cm) to water with specific conductance of about 1,078 μS/cm (EC+) and 2,039 μS/cm (EC++) to determine the effect of background salinity on the correlation coefficient. This was based

on reports regarding released hydrocarbons in coastal aquifers (Geng et al., 2017; Robinson et al., 2009). The ion compositions were determined by mixing a percentage of seawater (Nordstrom et al., 1979) with freshwater (initial concentration) using PHREEQC to reach the desired specific conductance.

PHC contaminated aquifers have varying dominant electron acceptors as reported for several sites (Colombani et al., 2009; Eckert & Appelo, 2002; Mastrocicco et al., 2012; Spence et al., 2005). Hence, we varied the dominant electron acceptor by removing the dissolved oxygen (DO0) from the initial level of 7.87 mg/L and removing the nitrate ($NO_3$0) and sulfate ($SO_4$0) from the initial levels of 5 and 50 mg/L, respectively. We also increased the nitrate level to 50 mg/L (NO_3+) (Fraters et al., 2008; European; Union, 2020), and the sulfate level to 250 mg/L (SO_4+) (European Union, 2020).

Carbonate minerals usually control the background concentration of ions in an aquifer because of their abundance in nature and high solubility in groundwater. The dissolution or precipitation of calcium carbonates in an aquifer matrix could affect the alkalinity and pH of groundwater, as well as the inorganic carbon concentration (Maurer & Rittmann, 2004). Hence, we also considered the absence of calcite (Cal0), reduced Fe $(OH)_3$ from 7.59 to 0.76 mmol/kg, and increased (CEC+) and decreased (CEC-) cation exchange capacities from 10.94 mol/kg to 2.19 mol/kg and 54.70 mol/kg. This is to evaluate the effect of minerals and the exchangeable cations on the correlation coefficients. The simulated scenarios are listed in Table S4 in Supporting Information S1.

2.7. Virtual Sampling of Groundwater

We obtained the concentration time series of simulated iWQP from eight virtual observation wells with screens at multiple depths (Figure 1). These wells, located at different depths and distances from the source zone, consisted of eight vertical grid cells from the top layer (1 m total length) and one horizontal grid cell (2 m diameter, minimum grid cell size).

The concentration at each virtual groundwater sample, C_{sample}, was calculated as the average of pumping flow-rate-weighted mean concentration at all the well grid cells to represent the well screen surroundings (Höyng et al., 2015). Assuming that the pumping flow rate is proportional to the hydraulic conductivity (Thouement & Van Breukelen, 2020), C_{sample} was computed as:

$$C_{\text{sample}} = \frac{\sum C_i K_i}{\sum K_i}, \tag{7}$$

where C_i is the species concentration and K_i is the hydraulic conductivity of the grid cell i. This method considered the influence of hydraulic conductivity on the groundwater flux toward the well screen during pumping (Thouement & Van Breukelen, 2020).

2.8. Statistical Data Analysis

We analyzed the relationships between iWQPs (DO, EC, ORP, and pH) and the PHCs (i.e., BEX and NVDOC). PhreeqPython, a Python implementation of PHREEQC (Vitens, 2021), was used to calculate the electrical conductivity based on the chemical water composition during post-processing. We then created histograms with kernel density estimation (KDE) and probability density function (PDF) plots for a descriptive overview of the distribution and frequency of the parameters.

Using Spearman's rank-order correlation, we quantified the association between the iWQPs and the PHCs at all observation wells. Spearman's correlation is a non-parametric measure that assesses the monotonic relationship between two variables (Sheskin, 2020). We then conducted a "moving window" analysis (Worrall et al., 2003), termed here as rolling Spearman's correlation analysis with a 5-year window, to capture temporal dynamics. Repeated calculations of the correlations allow for the identification of time-dependent patterns and shifts in correlation coefficients. The 5-year window was primarily chosen for illustrating the temporal dynamics inherent to the system. Finally, we assessed the effect of different simulated scenarios on the rolling Spearman's correlation by visualizing correlation coefficients between iWQPs and PHCs under various scenarios using heatmaps.

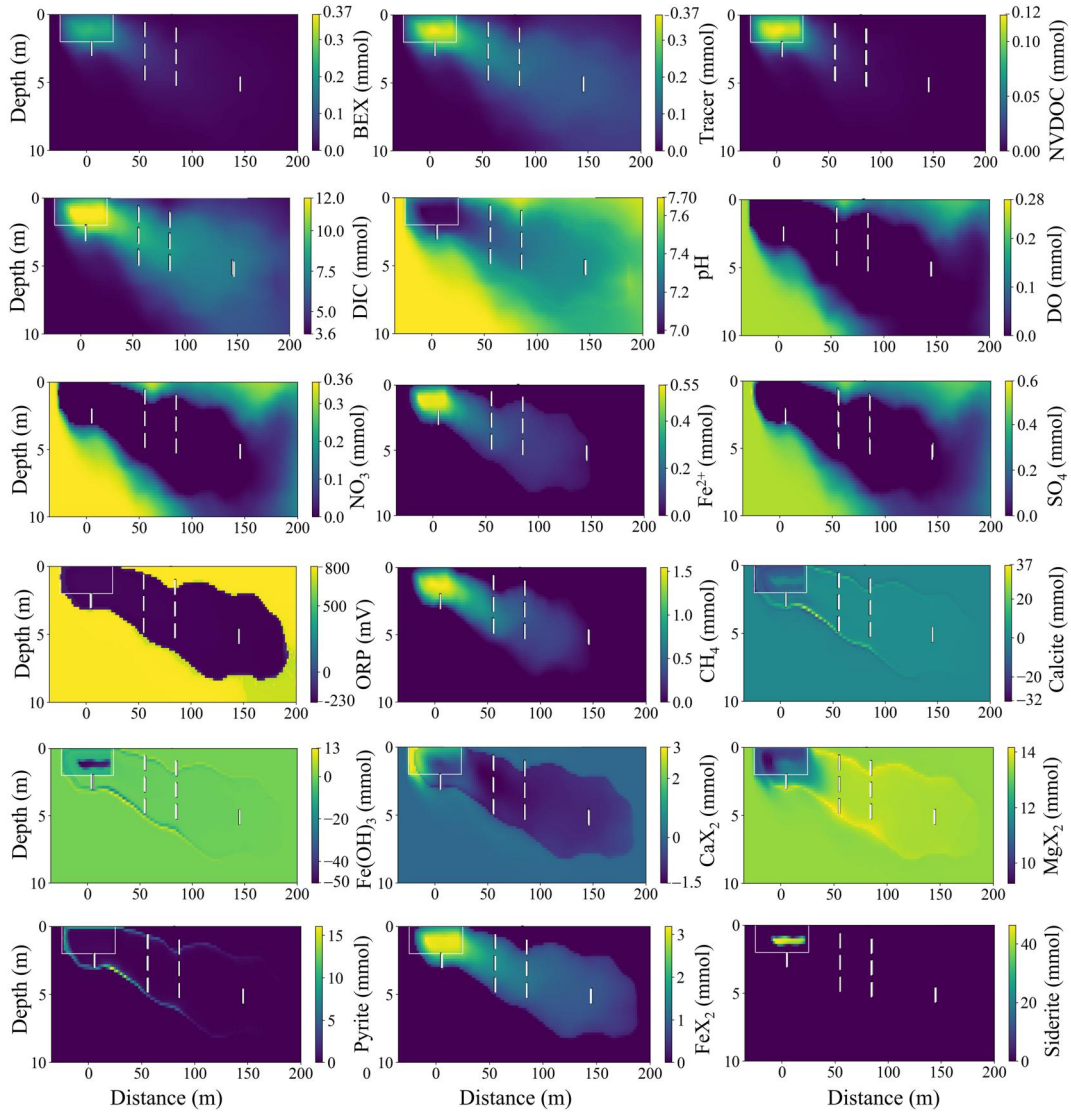

Figure 2. Model simulation results for major electron donors (BEX and NVDOC), the tracer representing BEX without degradation, DIC produced by all TEAPs, groundwater pH, depleted electron acceptors with redox zones development (ORP plume), solid phase minerals, and cation exchangers, after 30 simulation years. The solid phase plumes are depicted as the difference between the final and initial values. White rectangles delineate the source zone location.

3. Results and Discussion

3.1. Hydrogeochemistry of the Groundwater Pollution Plume

The leakage of petroleum hydrocarbons in the aquifer influenced the concentrations of aqueous phase constituents and solid phase minerals over time and space. We simulated the dissolution of petroleum hydrocarbons from a source zone (Figure 1), which triggered various terminal electron accepting processes (TEAPs). The total simulation period is 100 years, but we present the cross-sectional plumes after 30 years to approximately match the observation period at the Bemidji site (Ng et al., 2015). The plumes at three distinct time steps (5, 10, and 30 years) are presented in Figures S3 to S5 in Supporting Information S1 to visualize the plume progression.

3.1.1. Aqueous Phase Simulation Results

Figure 2 shows the cross-sectional plume simulations of major aqueous electron donors (BEX and NVDOC), a tracer representing BEX in the case of no degradation, dissolved inorganic carbon (DIC) produced by all

TEAPs, and the pH. The plumes of various electron acceptors and the redox zones development due to hydrocarbon degradation are also illustrated in Figure 2, along with the solid phase minerals and the cation exchangers (X represents a sorption site). In this figure, pH, DO, and ORP are the parameters measurable with water quality sensors. The location of the observation wells is displayed as vertical white lines, and the source zone is delineated by white rectangles. The model effectively simulated hydrocarbon dissolution, advection, and dispersion, as evident from BEX and NVDOC plume spreading. The results align with the previous study on the Bemidji site (Ng et al., 2015), although it has differences such as plume extent and concentration. Several factors contribute to the variability between our simulation results and those of the Bemidji plume such as differences in initial oil saturation, mineral composition, hydraulic conductivity field, transient groundwater flow, and the presence of nitrate and sulfate. Note that our purpose is to simulate a general hydrocarbon pollution plume inspired by the Bemidji case, but not to represent the exact situation as it was at the Bemidji site.

The findings of a report on a groundwater-contaminated site at a former gasworks plant in Düsseldorf, Germany (Eckert et al., 2000) demonstrate the feasibility of the simulated BEX concentration of more than 0.2 mmol/L (15.6 mg/L) and plume length of more than 100 m. The study by Eckert et al. (2000) reported PHC concentrations of up to 100 mg/L, with the plume extending to 600 m over a period of more than 50 years of natural attenuation. Comparing the extent of the BEX plume with that of the much larger tracer (BEX without decay) plume demonstrates hydrocarbon degradation. The degradation of all PHCs led to significant DIC and pH plumes stretching far beyond the hydrocarbon plumes (Ng et al., 2014, 2015). Note that the NVDOC levels increased considerably in the source zone over 30 years, whereas BEX levels remained largely similar.

The hydraulic conductivity of the aquifer significantly affects the characteristics of the hydrocarbon plume. A region of relatively high hydraulic conductivity (Figure 1) caused the plumes to initially migrate downward and then almost horizontal. Similarly, the shape of the PHC plume in a sandy aquifer near a petroleum oil and lubricant facility in Utah was also found to be sensitive to the hydraulic conductivity and aquifer thickness (Lu et al., 1999). Additionally, the geological heterogeneity enhanced the contaminant source dissolution in a controlled gasohol spill site in Brazil, resulting in greater plume migration (Rama et al., 2019). Furthermore, it was determined in a numerical model that the heterogeneity in hydraulic conductivity greatly affects the shape and size of the PHC plume (Uçankuş & Ünlü, 2008).

In aquifers, the release of carbonic acids from hydrocarbon degradation tends to decrease the pH of groundwater (Appelo & Postma, 2005; Pandolfo et al., 2023). This was simulated in the model by the oxidation of organic carbon through the partial equilibrium approach, where H^+ is produced in the TEAP. Examples are the aerobic degradation of benzene and NVDOC, respectively:

$$C_6H_6 + 3\ H_2O + 7.5\ O_2 \rightarrow\ 6\ HCO_3^- + 6\ H^+, \tag{8}$$

$$C_{19}H_{24}O_6 + 7\ H_2O + 22\ O_2 \rightarrow\ 19\ HCO_3^- + 19\ H^+, \tag{9}$$

which produce H^+ and HCO_3^- resulting to lower pH and higher DIC concentration, as observed in Figure 2. The possibility to detect PHC using pH and EC because of the increase in ions is based on this principle. Additionally, a fraction of the produced CO_2 from n-alkane degradation dissolves, providing an additional source of H^+. The simulation captures a low pH plume originating from the core of the source zone, reflecting the early and expanding low pH plume similarly observed at the Bemidji site (Ng et al., 2015). However, the previous study reported lower simulated pH values (below 7) due to an additional source of H^+ following their cation-exchange model.

The depletion of DO, NO_3, and SO_4, along with the release of Fe^{2+} also shown in Figure 2 demonstrates the conversion of organic carbon into inorganic carbon through kinetically controlled biodegradation. This process progressively consumes the oxidation capacity of both aqueous and mineral electron acceptors (Prommer & Post, 2010). Near the contamination source, DO was depleted shortly after a spill incident caused by the aerobic degradation of organic matter at the Bemidji site (Ng et al., 2015). This shows that DO sensors can be used to detect the presence of PHC. Note that the SO_4 depletion zones are smaller than those of O_2 and NO_3 because SO_4 is a less preferred electron-acceptor.

10.1029/2023WR036644

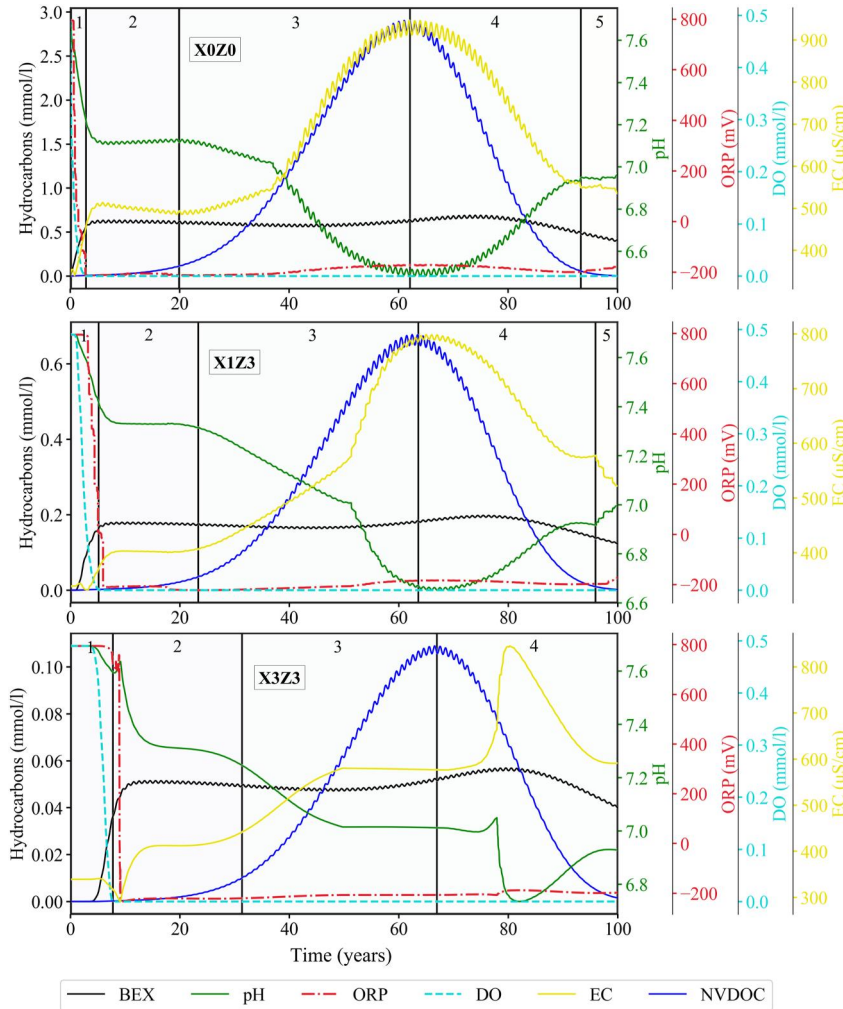

Figure 3. Simulation results of BEX, NVDOC and in-situ water quality parameters at three observation wells X0Z0 (top), X1Z3 (middle), and X3Z3 (bottom) for 100 years, divided into identified periods. BEX levels are multiplied by five for visualization.

Previous studies also proved that PHC degradation in contaminated aquifers has been coupled with NO_3 and SO_4 reduction (Colombani et al., 2009; Eckert & Appelo, 2002), and iron reduction (Mastrocicco et al., 2012; Miles et al., 2008). When the more favorable electron acceptors are completely utilized, fermentation of the PHCs can still occur. This leads to the partial oxidation of the carbon atoms to HCO_3^- and partial reduction of the carbon atoms to CH_4, as reported at contaminated aquifers (Lueders, 2017; Morris et al., 2013; Teramoto et al., 2020). The development in redox zones was simulated in the model as demonstrated by the change in redox potential (ORP) shown in Figure 3. Thus, ORP sensors could potentially detect PHC in groundwater especially when degradation affects the redox zones.

Following the model of Ng et al. (2015), we simulated concomitant Fe(III)-reduction and methanogenesis by using low $Fe(OH)_3$ solubility to produce CH_4 early as observed at the Bemidji site. This leads to higher CH_4 concentration at later times, but the partial equilibrium model addressed this by representing anaerobic oxidation of methane coupled with iron reduction (Amos et al., 2011; Ng et al., 2015). In general, long-distance transportation of reaction products such as methane through the aquifer is possible (Appelo & Postma, 2005), leading to an extensive CH_4 plume as shown Figure 3. The mineralization of PHCs also resulted to accumulation of CH_4, producing a larger CH_4 plume with higher concentration than BEX and NVDOC. However, CH_4 oxidizes at the fringes when CH_4-containing groundwater mixes with oxygenated water.

3.1.2. Solid Phase Simulation Results

Near the source zone, the degradation of PHCs dissolves calcite because of proton formation (Figure 2); denitrification dissolves less calcite because of a decrease in proton formation in the redox reaction. Calcite dissolution (simulated as equilibrium process) increases Ca and alkalinity and thus acts as a buffer for groundwater acidity and increases the EC. As oxygen and nitrate become depleted, the subsequent reductive dissolution of iron hydroxides released Fe^{2+} into the groundwater (Teramoto & Chang, 2019; Vencelides et al., 2007). Calcite also precipitated since iron reduction consumes protons, as illustrated by calcite formation at areas with low $Fe(OH)_3$.

The increased HCO_3^- and Fe^{2+} from PHC degradation coupled with reductive $Fe(OH)_3$ dissolution triggered siderite precipitation. Siderite can stabilize when the dissolved sulfide is depleted, allowing the Fe^{2+} concentration to increase sufficiently (Appelo & Postma, 2005). This process continuously removed Fe^{2+} from the solution and lowered the pH, further promoting $Fe(OH)_3$ dissolution and reduction (Ng et al., 2015).

Within the source zone, the cation exchange sites adsorbed the calcium ions (increased CaX_2 concentration), mobilizing Mg^{2+}, K^+, and Na^+ (Figure S6 in Supporting Information S1). However, the produced Fe^{2+} from iron-reduction was partial sorbed to the CEC (increased FeX_2) and mostly exchanged with CaX_2, releasing more Ca^{2+} to the water. CaX_2 is thus depleted in most of the plume, while FeX_2 is enriched. As observed at the Bemidji site, PHC oxidation increased the groundwater acidity. This in turn increased the levels of calcium and magnesium in groundwater in response to calcite dissolution (Amos et al., 2011; Bennet et al., 1993). The resulting mineral depletion/enrichment patterns, however, differed from the study at the Bemidji site (Ng et al., 2015). We included Ca sorption in our model which was omitted in the sorption model for the Bemidji site. We also simulated the extensive elevated Ca^{2+} plume reported at the Bemidji site, highlighting the significance of calcite dissolution in controlling the groundwater chemistry.

3.1.3. Effect of Hydrocarbon Degradation on In-Situ Water Quality

Figure 3 presents the PHC concentration and the iWQP at three observation wells located directly below (X0Z0) the source zone and at horizontal distances of 85 m (X1Z3) and 145 m (X3Z3) away from the source zone, following the general direction of groundwater flow. We analyzed the data of all observation wells, but for illustrative purposes, we chose to visualize the data from these three specific wells. We also multiplied the BEX levels by five only for visualization since BEX has much lower levels than NVDOC (less than 10x). It must be noted that the accuracy and resolution of sensors must be considered when interpreting the practical implications of these findings. There are sensors with accuracy and resolution of ±0.1 and ±0.01 for pH, ±5 and ±0.1 mV for ORP, ±0.5% (of reading) and ±0.1 µS/cm for EC, and ±0.1 and ±0.01 mg/L for DO (In-Situ, 2024). Thus, small variations in sensor data might be difficult to detect in real-life application.

The time series data in Figure 3 reveals five distinct periods. The first period, spanning the initial 2.5 simulation years for X0Z0 (Figure S7 in Supporting Information S1), consists of aerobic conditions with BEX as the primary electron donor. This is consistent with the approximate travel time of particles from the source zone to X0Z0 which is 2–4 years (Figure S8 in Supporting Information S1). During this period, DO was completely consumed, leading to a stepwise decrease in ORP from +800 mV (associated with the O_2/H_2O redox couple) to around −125 mV (associated with the CO_2/CH_4 redox couple) (McMahon et al., 2011). From the PHC degradation, H^+ and HCO_3^- were produced, leading to a slight increase in EC from around 340 to 440 µS/cm and a decrease of pH from about 7.7 to 7.2.

The second period is characterized by BEX still acting as the main electron donor, but under anaerobic conditions. In this period, the pH further decreased to 7.1, while the EC further increased to about 510 µS/cm. After approximately 20 years, the third period started which marks the transition from BEX to NVDOC as the primary electron donor in the source zone which aligns with observations at the Bemidji site (Ng et al., 2015). The NVDOC concentration peaked at 61 years proving that petroleum contamination can accumulate and persist in groundwater for decades (Pishgar et al., 2022). As the degradation process progressed, groundwater further acidified with pH reaching the minimum value of 6.5. This is because NVDOC degradation produces more H^+ than BEX degradation per molecule (Equations 8 and 9).

This caused the calcite to dissolve, further, increasing the EC to the maximum value of about 950 µS/cm. An important observation is that the extreme EC and pH values were reached in about 1 and 3 years, respectively after the peak concentration of NVDOC was observed. A possible reason for this is the delay between the migration of

NVDOC and its degradation by-products. Variation in reaction kinetics of the different hydrocarbons can also contribute to the lag time before the impact on water quality can be observed. For example, the first-order degradation coefficient of BEX is 0.31 (1/year) while for NVDOC it is 0.46 (1/year). The delay between the peak NVDOC concentration and the maximum values of EC and pH differs among observation wells, with a longer delay at the farthest well.

In the fourth period starting in year 61, the NVDOC concentration starts to decline from its peak, indicating the depletion of the NVDOC source, during which the pH increased to about 6.9 while the EC decreased to 560 μS/cm. ORP increased slightly during periods 3 and 4, possibly due to the mixing of water with different redox states in the observation well. The fifth and final period starts at approximately 91.5 simulation years until the end of simulation period. During this period, hydrocarbons are almost depleted leading to stabilization in iWQP, as illustrated at the end of the time series. However, the iWQPs have not returned to their initial levels suggesting that a century is insufficient to completely remove the impact of PHC contamination. These time periods provide valuable insights into the temporal variations of hydrocarbon degradation and their impact on iWQP. Although it was known that PHC degradation can influence these iWQPs, the changes to water quality parameters have not been quantified and used to estimate the concentration of PHC in groundwater. Hence, these findings could serve as the core logic for virtual sensor development.

The starting and ending times of these characteristic periods depend on the position of the observation well with respect to the source zone, and more specifically the groundwater travel times between the source zone and the wells. These differences can be observed from the data at three observation wells shown in Figure 3 and the approximate travel times based on particle tracking in Figure S8 in Supporting Information S1 (Pollock, 2017).

Period one ends at around year 5 for X1Z3, which is related to the approximate travel time of 4–6 years from the source zone to the well, and at around year 8 for X3Z3 with an approximate travel time of 8–10 years. Furthermore, data from observation well X3Z3 show that the presence of BEX was detected 2.5 years after the start of simulation, as compared to X0Z0 where BEX was detected within the first simulation year. The DO was completely consumed and the ORP dropped to −225 mV after about 6.8 years at X3Z3 while only about 2.5 at X0Z0. The change from BEX to NVDOC as the main electron donor was observed after approximately 31 years at X3Z3, although only after 20 years at X0Z0. The NVDOC concentration peaked at a simulation time of around 67 years, approximately 6 years later than at observation well X0Z0.

The travel time of PHCs from the source zone to the observation wells can be influenced by the aquifer's hydraulic and hydrologic properties (Fetter et al., 2018; Gupta & Yadav, 2020) as shown in Figure S8 in Supporting Information S1. At the farthest observation well X3Z3 (horizontal distance of 145 m from the source zone's center), a lag time of about 14 years was observed between the peak NVDOC concentration and the maximum EC value of about 850 μS/cm; the lowest observed pH value of 6.7 had a longer lag time of approximately 15.5 years.

Aside from the differences in travel times, we also found that the signal from the water table fluctuation was dampened as we move from well X0Z0 closest to the left boundary, to the farthest well (X3Z3). This dampening is especially noticeable for pH and EC (Figure 3) and is attributed to the aquifer's heterogeneity that attenuates the signal as the water moves through the system. This is commonly observed in amplitude attenuation of tide-induced groundwater level fluctuations with the rate controlled by the aquifer's hydrogeologic properties (Housego et al., 2021; Huang et al., 2015; Rotzoll & El-Kadi, 2008). For clear illustration, the signal attenuation for the BEX tracer at different wells is also presented in Figure S9 in Supporting Information S1. This shows that the location of the observation well plays an important role in observing the behavior of hydrocarbon contaminants and their effects on the iWQPs.

3.2. Exploratory Data Analysis of Simulation Results

Simulated NVDOC, pH, and EC values at observation well X0Z0 have a multimodal distribution. BEX is negatively skewed while NVDOC is positively skewed (Figure S10 in Supporting Information S1). Therefore, Spearman's rank correlation was used instead of Pearson's correlation for data analysis. Spearman's correlation determines the direction and strength of the monotonic relationship between variables, rather than the linear relationship measured by Pearson's correlation (Sheskin, 2020).

We analyzed 100 years of PHC and iWQP simulation data at eight observation wells (Figure 4). As anticipated, different observation wells displayed varying correlation coefficients due to the factors influencing the fate and

10.1029/2023WR036644

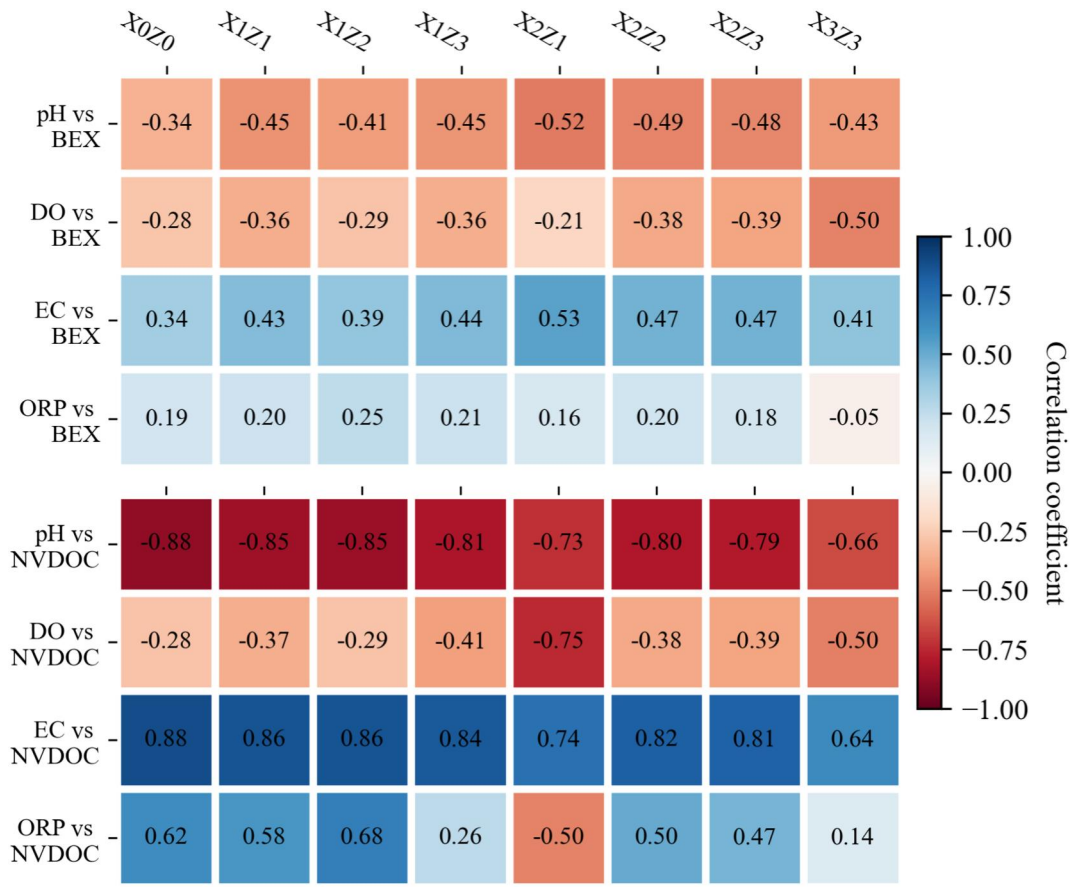

Figure 4. Correlation Coefficients between In-situ Water Quality Parameters and PHCs (BEX and NVDOC) at all Observation Wells with Well Locations for the 100 Years of Simulation Results). All correlations are statistically significant, p-value <0.05.

transport of contaminants, as discussed earlier. The correlations between the iWQP and NVDOC were generally stronger than those with BEX, except for DO which exhibited similar correlations. At 95% significance level, pH demonstrated a strong to very strong negative correlation with NVDOC (−0.66 to −0.89) and a moderate negative correlation with BEX (−0.34 to −0.52). Conversely, ORP displayed a moderate positive correlation with NVDOC, except at wells X2Z1 and X3Z3 where the correlation weakened. ORP also had a weak positive correlation with BEX, except at well X3Z3 where the correlation was negligible (0.08). The early consumption of DO result in weak negative correlations with both BEX and NVDOC. EC, however, exhibited weak to moderate positive correlations with BEX and strong to very strong positive correlations with NVDOC. These correlation coefficients support the previous discussions, confirming that the degradation of PHCs significantly influences groundwater pH and EC.

The negative PHC-pH and positive PHC-EC correlations are consistent with the increase in H^+ and HCO_3^-, thus lowering pH and increasing EC, due to PHC degradation. As more PHCs are being dissolved and degraded in groundwater, more calcite is also being dissolved, increasing the EC further. In contrast, the positive PHC-ORP correlation is inconsistent with the previous discussion where groundwater contamination of PHC typically results in a more reduced condition (lower ORP). This is because the most reduced condition was reached after approximately 2.5 years, followed by relatively stable ORP values. Thus, the correlation coefficients based on the 100-year simulation data do not accurately represent the actual correlation. We therefore considered the temporal variability of the data aside from spatial variability.

Figure 5 presents the values of Spearman's rolling correlation coefficients, with 5-year window, between the PHCs (BEX, NVDOC, and combined) and iWQP (pH and EC) at observation well X0Z0. Focus was given to pH and EC since DO was depleted after 2.5 years, resulting in methanogenic conditions (ORP of −220 mV). For the

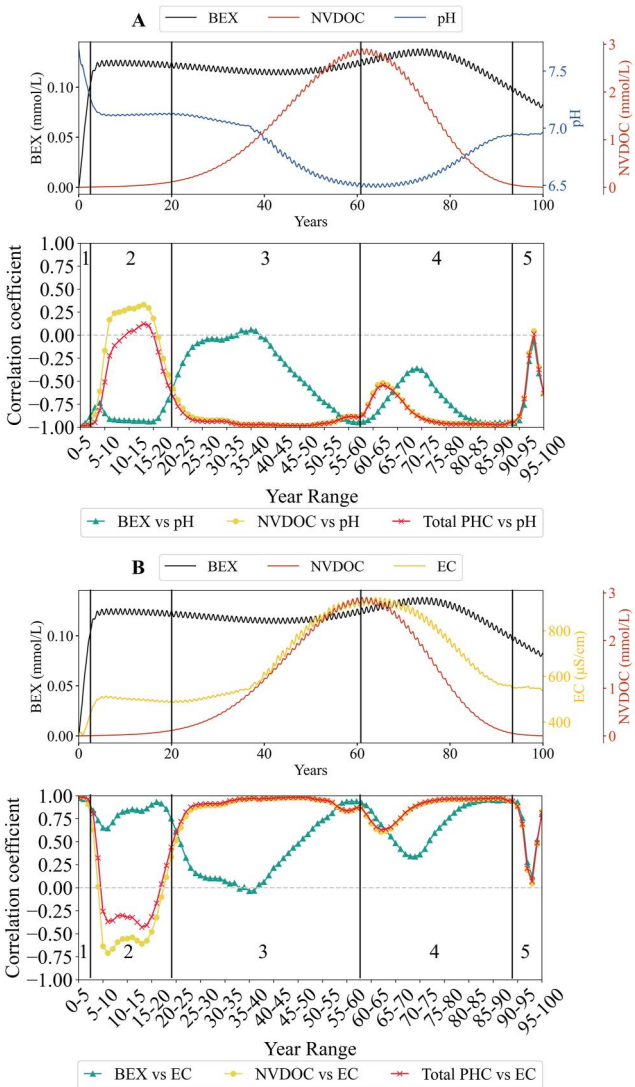

Figure 5. Spearman's rolling correlation with 5-year window of PHCs (BEX, NVDOC, and combined) versus pH (anel A) and EC (panel B) at observation well X0Z0 below the LNAPL source.

first 2 years, DO and ORP have a very strong negative correlation with both BEX and NVDOC (Spearman's r of −1 and −0.95, respectively) as previously anticipated, and thus not included in the illustration.

Figure 5 illustrates the five different phases observed at well X0Z0. During period 1, strong negative BEX-pH and NVDOC-pH correlations were observed, while EC exhibited a strong positive correlation. In period 2, pH and EC started to correspond with BEX (Spearman's r of about −0.8 and 0.8, respectively) more than NVDOC (Spearman's r of around 0.3 and −0.6, respectively). This shift can be attributed to BEX being the main electron donor in this period. Additionally, the positive NVDOC-pH correlation may suggest a slight pH buffering effect due to calcite dissolution.

The transition of the main electron donor from BEX to NVDOC at period 3 (Figure 5) notably reduced the BEX-pH and BEX-EC correlations and substantially increased the NVDOC-pH and NVDOC-EC correlations. This is because the peak NVDOC concentration was around 2.9 mmol/L, as compared to the BEX concentration of 0.14 mmol/L. The decline of NVDOC in period 4 caused a point of inflection in the correlation coefficients at around 60–65-year range (Figure 5), but still maintained a strong correlation with pH and EC until the beginning of period 5. From period 3 to period 5, the NVDOC-pH and total PHC-pH correlations behaved similarly, as well as with EC. It is worth noting that although period 3 was delineated based on NVDOC being the dominant PHC, the effect of increasing NVDOC concentration can already be observed at the end of period 2 where the BEX-pH and BEX-EC correlation coefficients started to decrease. These findings were also observed in the other wells. This includes the transition in the primary electron donor from BEX to NVDOC, and the switch between positive and negative correlations during certain periods.

3.3. Influence of Different Scenarios on the Correlation Coefficients

The possible effects of various conditions on the correlation between PHC and iWQP were investigated. These factors have been known to influence the transport of ions and contaminants in groundwater, as well as the TEAPs and pH buffering capacity of the aquifer, among others. The Spearman's rolling correlation coefficients of PHCs (BEX and NVDOC) versus pH and EC at observation well X0Z0 for different scenarios are presented in Figure 6. As we have seen, focus was given to pH and EC since after 2.5 years, DO was depleted resulting in a reduced aquifer condition. Identified periods from the base case scenario are visually delineated by black vertical lines within the figure for comparison with other scenarios.

The increased amplitude of WF to 0.75 (WF++) slightly decreased the BEX-pH and BEX-EC correlations during period 1 (lighter colors) but increased these correlations in period 2. Periods 3, 4, and 5 also exhibited an overall increase in correlation, particularly evident at the beginning of period 3. For NVDOC, the correlations decreased during period 2 but showed varying effects across periods 3, 4, and 5. The increased WF has varying effects on the correlation coefficients, suggesting that the synchrony between time series data of PHC and iWQPs was altered. WF has been found to affect the transport of species in groundwater including PHCs, inducing temporal and spatial variations in aquifer conditions (Abbas et al., 2017; Alazaiza et al., 2020).

When the hydraulic conductivity was lowered (HK-), the BEX-pH and BEX-EC correlations increased during period 1, at the beginning of period 2, and during period 5. Interestingly, instances of reversed correlations can be found across periods 2, 3, and 4. Red changed to blue for pH, while blue changed to red for EC. The change in groundwater flow velocity due to lower (HK-) and higher hydraulic conductivity (HK+) caused the pH and EC to correspond more with NVDOC (darker color) than BEX (lighter color). The change in groundwater velocity due to changes in HK also affected the timing of the different periods such as longer period 1 at the HK- scenario.

10.1029/2023WR036644

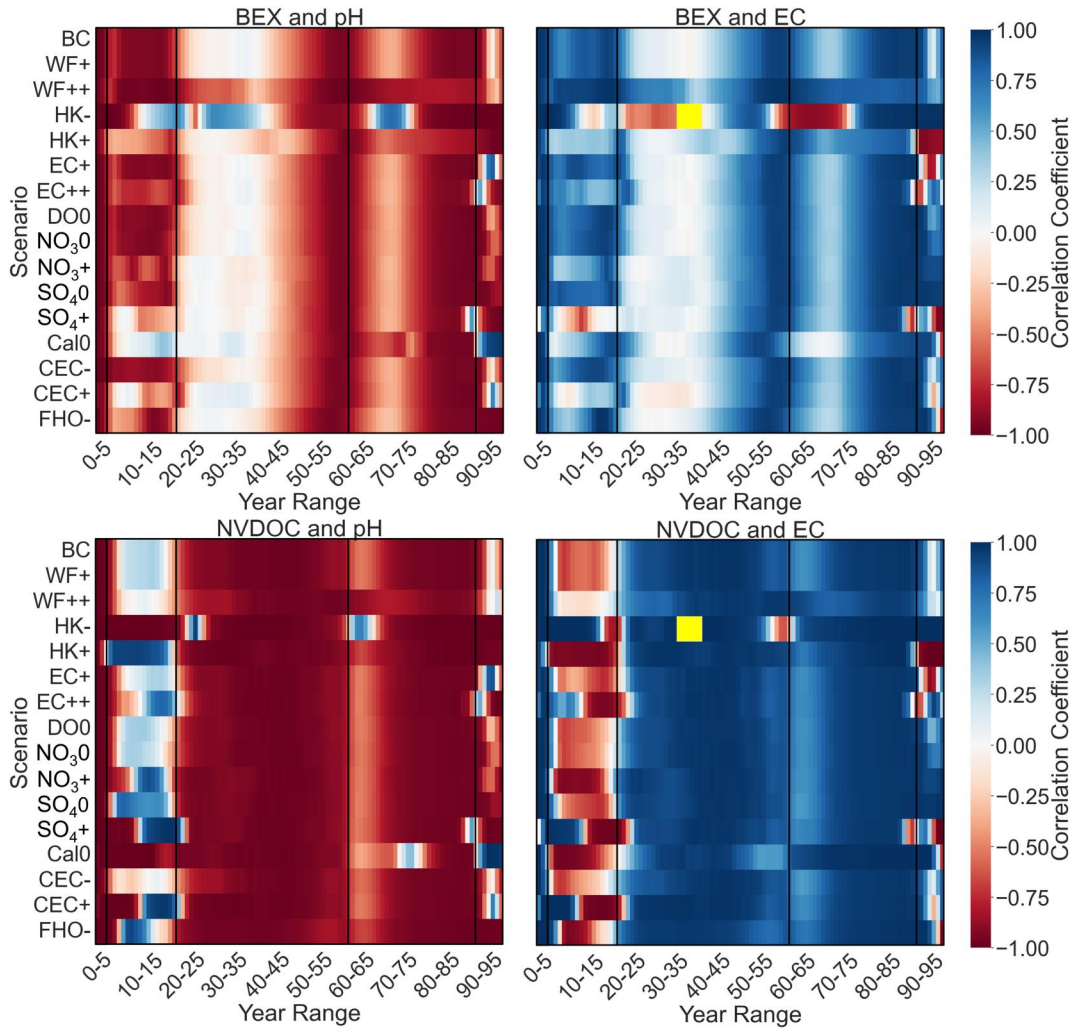

Figure 6. Spearman's rolling correlation with 5-year window of PHCs (BEX and NVDOC) versus iWQP (pH and EC) at observation well X0Z0 for different scenarios (BC: base case, WF: water table fluctuation, HK: hydraulic conductivity, EC: electrical conductivity, DO: dissolved oxygen, NO_3: nitrate, SO_4: sulfate, Cal: calcite, CEC: cation exchange capacity, FHO: amorphous ferric hydroxide). Parameters were changed relative to BC (+ for increased, - for decreased, 0 for removed). Yellow rectangles mark the period with no EC data. Values changed are presented in Table S4 in Supporting Information S1.

Slower groundwater flow led to slower transport of PHC from the source zone to the observation well, resulting to longer time before the DO was depleted. It must be noted that PhreeqPython failed to calculate the EC between 30–5 and 40–45-year range at the HK- scenario, marked as yellow rectangles, as can be observed in Figure 6. This could be caused by the adapted virtual sampling method, where the HK was used for calculating the species concentration at the observation wells.

The elevated background EC (EC+) slightly decreased the BEX-EC correlation during period 1 but increased it during period 5. The correlation at periods 1 and 2 further decreased with much higher background EC (EC++), which also affected the BEX-pH correlation, more noticeably during period 1. Higher background EC values reduced the noticeability of the signal from BEX contamination, causing this decrease in correlation (lower signal-to-noise ratio). NVDOC-pH and NVDOC-EC correlations exhibited the opposite effect, resulting in an increased correlation in the EC++ scenario mostly at period 2. This shows that the change in EC caused by NVDOC is significant even at high background EC.

Since oxygen, nitrate, and sulfate are important mainly during the initial periods (until these are exhausted), the BEX-pH and BEX-EC correlations remained relatively stable when DO and nitrate were removed (DO0 and $NO_3$0, respectively), with a slight decrease when sulfate was removed ($SO_4$0). However, increasing the nitrate

and sulfate levels (NO_3+ and SO_4+, respectively) decreases the BEX-pH correlation significantly at period 2 while increasing the NVDOC-pH and NVDOC-EC correlations; SO_4+ also altered the direction of BEX-EC correlation at period 2, end of period 4, and period 5. By varying the available electron acceptors, the timing of the periods could also change since each period is affected by the presence of the main electron acceptor.

When the system has no calcite (Cal0), the BEX-pH and BEX-EC correlations significantly decreased causing the periods to be indistinguishable. Since pH was not buffered because of the absence of calcite, pH correlated more with NVDOC. Without calcite, the pH dropped more than 0.7 as compared to the base case while the EC increased more than 350 μS/cm at certain periods. Degradation of NVDOC (Equation 9) produces more H^+ than BEX (Equation 8), thus without buffering, NVDOC controls the groundwater pH. Decreasing the cation exchange capacity (CEC-) did not significantly impact the correlations, except for NVDOC-pH, which showed a slight increase in correlation during period 2. Increasing the cation exchange capacity (CEC+) reduced both the BEX-pH and BEX-EC correlations. For the NVDOC-pH and NVDOC-EC correlations, these were either increased during period 2, or period 1 became longer.

A reduction in amorphous iron oxide (FHO-) had a significant effect on the correlations during period 2 and period 5. It decreased both BEX-pH and BEX-EC correlations in period 2 but increased the BEX-pH, BEX-EC, NVDOC-pH, and NVDOC-EC correlations in both periods. As previously discussed, iron oxides play a role in reductive mineral dissolution, precipitation, and cation exchange. Thus, reducing its availability impacted these processes leading to different correlation coefficients. This shows the importance of iron oxides in characterizing groundwater quality with PHC contamination (Jiang et al., 2019). In general, increasing the electron acceptors can significantly affect the correlations between PHCs and iWQPs. The correlation coefficients were notably affected in period 2 and period 5. These periods correspond to a phase before a transition between electron donors occurs, highlighting the significance of TEAPs in characterizing these relationships. In contrast, the correlation coefficients in period 4 remained relatively stable except for major changes during scenarios HK- and Cal0. Furthermore, a decrease in BEX-pH or BEX-EC correlations is typically accompanied by an increase in NVDOC-pH or NVDOC-EC correlations, and vice versa.

3.4. Implications for Virtual Sensor Development

Virtual sensors use models to process and transform physical sensor data into signals of interest (Brunello et al., 2021; Martin et al., 2021), such as PHC concentration. In contrast to RTM where the input parameters include the aquifer chemistry and the PHC, the input parameters for the hydrocarbon virtual sensor will only be the iWQPs; we expect the virtual sensor to detect and estimate the concentration of PHC in groundwater by combining these iWQPs. The correlation between the physical sensor data and the PHC concentration must therefore be determined to identify the most suitable process for virtual sensor development. Since the correlation coefficients have been found to have temporal dependencies causing varying lag times between PHC contamination and changes in water quality, at least two different virtual sensor systems can be conceptualized. These systems will vary in terms of purpose and the processing of sensor data; these will be the focus of future research and are not within the scope of this paper.

First is an early warning system utilizing the initial years following an oil spill (period 1). During the period when the condition is aerobic, PHC concentration has a perfect negative correlation with DO and ORP, making these parameters invaluable for early PHC detection. This system can be used to detect PHC contamination in real-time allowing for a quick remediation response, and thus preventing the PHC plume from spreading. Second is a system for long-term monitoring of PHC-contaminated aquifer, considering periods after period 1. EC and pH play important roles during these periods as these provide insights into the crucial chemical processes in groundwater. As the correlation coefficients differ per period due to variations in available electron acceptor and elector donors, among others, this system must have a mechanism for selectively updating the model based on the period that is monitored. This low-cost, low-maintenance, and continuous monitoring of PHC concentration in contaminated areas can be useful for developing effective and efficient remediation strategies across the lifespan of the plume. These findings serve as an essential intellectual footing for developing a robust hydrocarbon virtual sensor.

Hydrogeological properties of the aquifer were also found to affect the correlation coefficients. Figure 6 shows that the coefficients change in the identified periods, and that the timing and duration of each period change. Thus, aquifer characteristics and geochemical conditions such as hydraulic conductivity and available minerals are

important considerations when developing the virtual sensors. Other factors which were beyond the scope of this study might also affect the correlation coefficients and thus must be further studied. These factors include the source zone dimensions, heterogeneity in background aquifer chemistry, and hydrocarbon sorption on sedimentary organic matter. Field applications must also account for noises present in the data due to possible natural variations in groundwater conditions. Moreover, sensor accuracy, precision, and stability should be considered; small fluctuations in simulated water quality parameters were considered in the statistical analysis but may not be within the sensors' precision which can potentially result to weaker correlation coefficients.

4. Conclusions

This study investigated the potential of in-situ water quality sensors for estimating petroleum hydrocarbons (PHC) in groundwater. We developed a reactive transport model to generate synthetic data sets, which were essential toward creating a virtual sensor to detect PHC in groundwater. Our exploratory and statistical data analysis reveals that several factors influence the correlation between in-situ water quality parameters (iWQPs) and PHCs. These correlation coefficients exhibit spatial and temporal variability among observation wells and among the five identified periods in the base case scenario. Scenario simulations revealed the impact of various factors, including water table fluctuations, hydraulic conductivity, aqueous and mineral phase electron acceptors, and other geochemical properties of the aquifer, on the correlation between PHCs and iWQPs. These findings demonstrate the feasibility of developing two virtual sensor systems: an early warning system for rapid responses to oil leakages affecting groundwater; and a continuous, real-time, long-term monitoring system aimed at devising effective remediation strategies for PHC-contaminated aquifers.

Data Availability Statement

The reactive transport model in this paper was built in Jupyter Notebook using the Python package Flopy. The Jupyter Notebook is preserved at 4TU.ResearchData repository https://doi.org/10.4121/f7742f02-ee3a-4a84-adf1-625b4a9fd703 (Wu, 2024). The Jupyter Notebook and the python module created to visualize the simulation results are also available at this repository, as well as Databases S1 and S2 in Supporting Information S1. The software/code repository for Flopy is available at https://github.com/modflowpy/flopy (Bakker et al., 2024). Electrical conductivity was calculated using PhreeqPython licensed under the Apache License, version 2.0, available at https://github.com/Vitens/phreeqpython (Vitens, 2021). Figures were made with Matplotlib version 3.7.1 (Caswell et al., 2020; Hunter, 2007), available under the Matplotlib license at https://matplotlib.org/. Statistical analyses were done with SciPy version 1.10.1 (Virtanen et al., 2020).

Acknowledgments

This work has been performed within the cooperation framework of Wetsus, the European Centre of Excellence for Sustainable Water Technology (wetsus.nl), and Delft University of Technology (tudelft.nl). Wetsus is co-funded by the Dutch Ministry of Economic Affairs, the Ministry of Infrastructure and Environment, the European Union Regional Development Fund, the Northern Netherlands Provinces, and the Province of Fryslân. We would like to thank the participants of the "Sensoring" theme for the informative discussions and financial support, Crystal Ng for providing the modified PHT3D database, and Haruko Wainwright for giving a positive and constructive review of this paper. This research has been financially supported by the Netherlands Organization for Scientific Research (NWO; Sustainable Water Technology Call 2018; contract number: ALWET.2019.003).

References

Abbas, M., Jardani, A., Soueid Ahmed, A., Revil, A., Brigaud, L., Bégassat, P., & Dupont, J. P. (2017). Redox potential distribution of an organic-rich contaminated site obtained by the inversion of self-potential data. *Journal of Hydrology*, *554*, 111–127. https://doi.org/10.1016/J.JHYDROL.2017.08.053

Alazaiza, M. Y. D., Ramli, M. H., Copty, N. K., Sheng, T. J., & Aburas, M. M. (2020). LNAPL saturation distribution under the influence of water table fluctuations using simplified image analysis method. *Bulletin of Engineering Geology and the Environment*, *79*(3), 1543–1554. https://doi.org/10.1007/S10064-019-01655-3/FIGURES/10

Amos, R. T., Bekins, B. A., Delin, G. N., Cozzarelli, I. M., Blowes, D. W., & Kirshtein, J. D. (2011). Methane oxidation in a crude oil contaminated aquifer: Delineation of aerobic reactions at the plume fringes. *Journal of Contaminant Hydrology*, *125*(1–4), 13–25. https://doi.org/10.1016/j.jconhyd.2011.04.003

Amos, R. T., Mayer, K. U., Bekins, B. A., Delin, G. N., & Williams, R. L. (2005). Use of dissolved and vapor-phase gases to investigate methanogenic degradation of petroleum hydrocarbon contamination in the subsurface. *Water Resources Research*, *41*(2), 1–15. https://doi.org/10.1029/2004WR003433

Anderson, M. P., Woessner, W. W., & Hunt, R. J. (2015). APPLIED MODELING simulation of flow and advective transport (2nd ed.).

Appelo, C. A. J., & Postma, D. (2005). Geochemistry, groundwater and pollution, second edition. *Geochemistry, Groundwater and Pollution*, 1–649. https://doi.org/10.1201/9781439833544

Aronson, D., Citra, M., Shuler, K., Printup, H., Howard, P. H., & Weber, E. J. (1999). Aerobic biodegradation of organic chemicals in environmental media: A summary of field and laboratory studies.

Ayscough, N. J., Young, W., Whitehouse, P., & AgencyBritain, G. E. (2002). *Proposed environmental quality standards for ethylbenzene in water*. Environment Agency.

Baedecker, M. J., Eganhouse, R. P., Bekins, B. A., & Delin, G. N. (2011). Loss of volatile hydrocarbons from an LNAPL oil source. *Journal of Contaminant Hydrology*, *126*(3–4), 140–152. https://doi.org/10.1016/J.JCONHYD.2011.06.006

Bakker, M. (2019). Analytic solutions for tidal propagation in multilayer coastal aquifers. *Water Resources Research*, *55*(4), 3452–3464. https://doi.org/10.1029/2019WR024757

Bakker, M., & Post, V. (2022). Analytical groundwater modeling: Theory and applications using python analytical groundwater modeling: Theory and applications using Python. *ANALYTICAL-GROUNDWATER-MODELING-MARK-BAKKER-VINCENT-POST*, 1–226. https://doi.org/10.1201/9781315206134/

Bakker, M., Post, V., Hughes, J. D., Langevin, C. D., White, J. T., Leaf, A. T., et al. (2024). FloPy v3.7.0.dev0 (preliminary): U.S. Geological Survey software release, 08 february 2024 [Software]. *GitHub*. https://doi.org/10.5066/F7BK19FH

Bakker, M., Post, V., Langevin, C. D., Hughes, J. D., White, J. T., Starn, J. J., & Fienen, M. N. (2016). Scripting MODFLOW model development using Python and FloPy. *Ground Water*, *54*(5), 733–739. https://doi.org/10.1111/GWAT.12413

Beckett, G. D., & Lundegard, P. (1997). *Practically impractical - the limits of LNAPL recovery and relationship to risk*. Ground Water Publishing Co.

Bender, F., Mohler, R., Ricco, A. J., & Josse, F. (2012). Quantification of benzene in groundwater using SH-surface acoustic wave sensors. https://doi.org/10.5162/IMCS2012/5.4.2

Bennett, P. C., Siegel, D. E., Baedecker, M. J., & Holt, M. F. (1993). Crude oil in a shallow sand and gravel aquifer-l. Hydrogeology and inorganic geochemistry. In *Applied geochemistry* (Vol. 8).

Brunello, A., Urgolo, A., Pittino, F., Montvay, A., & Montanari, A. (2021). Virtual sensing and sensors selection for efficient temperature monitoring in indoor environments. *Sensors*, *21*(8), 2728. https://doi.org/10.3390/s21082728

Buerck, J., Roth, S., Kraemer, K., Scholz, M., & Klaas, N. (2001). Application of a fiber-optic NIR-EFA sensor system for in situ monitoring of aromatic hydrocarbons in contaminated groundwater. *Journal of Hazardous Materials*, *83*(1–2), 11–28. https://doi.org/10.1016/S0304-3894(00)00335-6

Caswell, T. A., Droettboom, M., Lee, A., Hunter, J., Firing, E., Sales De Andrade, E., & Ivanov, P. (2020). matplotlib/matplotlib: Rel: v3. 3.1 [Software]. *Zenodo*. https://matplotlib.org/

Cavelan, A., Golfier, F., Colombano, S., Davarzani, H., Deparis, J., & Faure, P. (2022). A critical review of the influence of groundwater level fluctuations and temperature on LNAPL contaminations in the context of climate change. In *Science of the total environment* (Vol. 806). Elsevier B.V. https://doi.org/10.1016/j.scitotenv.2021.150412

Chiang, W.-H., & Kinzelbach, W. (2003). Your first groundwater model with PMWIN. *3D-Groundwater Modeling with PMWIN*, 7–53. https://doi.org/10.1007/978-3-662-05549-6_2

Colombani, N., Mastrocicco, M., Gargini, A., Davis, G. B., & Prommer, H. (2009). Modelling the fate of styrene in a mixed petroleum hydrocarbon plume. *Journal of Contaminant Hydrology*, *105*(1–2), 38–55. https://doi.org/10.1016/j.jconhyd.2008.11.005

Cozzarelli, I. M., Schreiber, M. E., Erickson, M. L., & Ziegler, B. A. (2016). Arsenic cycling in hydrocarbon plumes: Secondary effects of natural attenuation. *Arsenic Cycling in Hydrocarbon Plumes: Secondary Effects of Natural Attenuation*, *54*(1), 35–45. https://doi.org/10.1111/gwat.12316

D'Affonseca, F. M., Prommer, H., Finkel, M., Blum, P., & Grathwohl, P. (2011). Modeling the long-term and transient evolution of biogeochemical and isotopic signatures in coal tar-contaminated aquifers. *Water Resources Research*, *47*(5). https://doi.org/10.1029/2010WR009108

Dillard, L. A., Essaid, H. I., & Herkelrath, W. N. (1997). Multiphase flow modeling of a crude-oil spill site with a bimodal permeability distribution. *Water Resources Research*, *33*(7), 1617–1632. https://doi.org/10.1029/97WR00857

Domenico, P. A., & Schwartz, F. W. (1998). *Physical and chemical hydrogeology* (2nd ed.). John Wiley and Sons, Inc.

Eckert, P., & Appelo, C. A. J. (2002). Hydrogeochemical modeling of enhanced benzene, toluene, ethylbenzene, xylene (BTEX) remediation with nitrate. *Water Resources Research*, *38*(8), 1–11. https://doi.org/10.1029/2001wr000692

Eckert, P., Wisotzky, F., Obermann, P., Kracht, O., & Strauss, H. (2000). Natural bioattenuation and active remediation in a BTEX contaminated aquifer in Düsseldorf (Germany). *Ground Water*, 389–390. https://doi.org/10.1201/9781003078593-192

Erickson, T. A., & Lear, K. L. (2014). An integrated optoelectronic chip for sensing aromatic hydrocarbon contaminants in groundwater. *Sensors and Actuators B: Chemical*, *204*, 421–428. https://doi.org/10.1016/J.SNB.2014.06.020

Essaid, H. I., Bekins, B. A., Godsy, E. M., Warren, E., Baedecker, M. J., & Cozzarelli, I. M. (1995). Simulation of aerobic and anaerobic biodegradation processes at a crude oil spill site. *Water Resources Research*, *31*(12), 3309–3327. https://doi.org/10.1029/95wr02567

Essaid, H. I., Cozzarelli, I. M., Eganhouse, R. P., Herkelrath, W. N., Bekins, B. A., & Delin, G. N. (2003). Inverse modeling of BTEX dissolution and biodegradation at the Bemidji, MN crude-oil spill site. *Journal of Contaminant Hydrology*, *67*(1–4), 269–299. https://doi.org/10.1016/S0169-7722(03)00034-2

European Commission (2001). MTBE and the requirements for underground storage tank .ec. · PDF fileMTBE and the requirements for underground storage tank construction and operation in member states A report - [PDF document]. Retrieved from https://fdocuments.net/document/mtbe-and-the-requirements-for-underground-storage-tank-eceuropaeuenvironmentairpdffuturetransportpdfpdf.html?page=1

Fetter, C. W., Charles, W., Boving, T. B., & Kreamer, D. K. (2018). Contaminant hydrogeology. *647*.

Fraters, B., Boumans, L. J. M., Van Elzakker, B. G., Gast, L. F. L., Griffioen, J., Klaver, G. T., et al. (2008). A new compliance checking level for nitrate in groundwater? *Feasibility study on monitoring the upper five metres of groundwater*. www.rivm.nl

Freitas, J. G., Doulatyari, B., Molson, J. W., & Barker, J. F. (2011). Oxygenated gasoline release in the unsaturated zone, Part 2: Downgradient transport of ethanol and hydrocarbons. *Journal of Contaminant Hydrology*, *125*(1–4), 70–85. https://doi.org/10.1016/j.jconhyd.2011.05.002

Geng, X., Boufadel, M. C., & Cui, F. (2017). Numerical modeling of subsurface release and fate of benzene and toluene in coastal aquifers subjected to tides. *Journal of Hydrology*, *551*, 793–803. https://doi.org/10.1016/J.JHYDROL.2016.10.039

Gharedaghloo, B., & Price, J. S. (2021). Assessing benzene and toluene adsorption with peat depth: Implications on their fate and transport. *Environmental Pollution*, *274*, 116477. https://doi.org/10.1016/J.ENVPOL.2021.116477

Gomez, D. E., & Alvarez, P. J. J. (2010). Comparing the effects of various fuel alcohols on the natural attenuation of Benzene Plumes using a general substrate interaction model. *Journal of Contaminant Hydrology*, *113*(1–4), 66–76. https://doi.org/10.1016/j.jconhyd.2010.02.002

Gupta, P. K., & Yadav, B. K. (2020). Three-dimensional laboratory experiments on fate and transport of LNAPL under varying groundwater flow conditions. *Journal of Environmental Engineering*, *146*(4), 4020010. https://doi.org/10.1061/(asce)ee.1943-7870.0001672

Hadley, P. W., Arulanantham, R., & Gandhi, D. (2015). California's low-threat LUFT site closure policy: Looking forward. *Remediation Journal*, *25*(2), 9–33. https://doi.org/10.1002/REM.21421

Harbaugh, A. W. (2005). MODFLOW-2005, the U.S. Geological Survey modular ground-water model-the ground-water flow process. Retrieved from http://water.usgs.gov/software/ground_water.html/

Healy, R. W., & Cook, P. G. (2002). Using groundwater levels to estimate recharge. *Hydrogeology Journal*, *10*(1), 91–109. https://doi.org/10.1007/S10040-001-0178-0/METRICS

Housego, R., Raubenheimer, B., Elgar, S., Cross, S., Legner, C., & Ryan, D. (2021). Coastal flooding generated by ocean wave- and surge-driven groundwater fluctuations on a sandy barrier island. *Journal of Hydrology*, *603*, 126920. Part B. https://doi.org/10.1016/j.jhydrol.2021.126920

Höyng, D., Prommer, H., Blum, P., Grathwohl, P., & Mazo D'Affonseca, F. (2015). Evolution of carbon isotope signatures during reactive transport of hydrocarbons in heterogeneous aquifers. *Journal of Contaminant Hydrology*, *174*, 10–27. https://doi.org/10.1016/J.JCONHYD.2014.12.005

Huang, F., Chuang, M., Wang, G. S., & Yeh, H. (2015). Tide-induced groundwater level fluctuation in a U-shaped coastal aquifer. *Journal of Hydrology*, *530*, 291–305. https://doi.org/10.1016/j.jhydrol.2015.09.032

Hunter, J. D. (2007). Matplotlib: A 2D graphics environment. *Computing in Science and Engineering*, *9*(3), 90–95. https://doi.org/10.1109/MCSE.2007.55

Huntley, D., Hawk, R. N., & Corley, H. P. (1994). Nonaqueous phase hydrocarbon in a fine-grained sandstone: 1. Comparison between measured and predicted saturations and mobility. *Ground Water*, *32*(4), 626–634. https://doi.org/10.1111/J.1745-6584.1994.TB00898.X

In-Situ (2024). Aqua TROLL multiparameter sondes. Retrieved from https://in-situ.com/pub/media/support/documents/Aqua-TROLL-500-600-700-800_Spec-Sheet_ltr_en.pdf

Jakobsen, R., & Postma, D. (1999). Redox zoning, rates of sulfate reduction and interactions with Fe-reduction and methanogenesis in a shallow sandy aquifer, Rømø, Denmark. *Geochimica et Cosmochimica Acta*, *63*(1), 137–151. https://doi.org/10.1016/S0016-7037(98)00272-5

Jiang, X. W., Sun, Z. C., Zhao, K. Y., Shi, F. S., Wan, L., Wang, X. S., & Shi, Z. M. (2017). A method for simultaneous estimation of groundwater evapotranspiration and inflow rates in the discharge area using seasonal water table fluctuations. *Journal of Hydrology*, *548*, 498–507. https://doi.org/10.1016/J.JHYDROL.2017.03.026

Jiang, Y., Xi, B., Li, R., Li, M., Xu, Z., Yang, Y., & Gao, S. (2019). Advances in Fe(III) bioreduction and its application prospect for groundwater remediation: A review. *Frontiers of Environmental Science & Engineering*, *13*(6), 1–11. https://doi.org/10.1007/S11783-019-1173-9/METRICS

Kabadayi, S., Pridgen, A., & Julien, C. (2006). Virtual sensors: Abstracting data from physical sensors.

Kulkarni, P. R., Newell, C. J., King, D. C., Molofsky, L. J., & Garg, S. (2020). Application of four measurement techniques to understand natural source zone depletion processes at an LNAPL site. *Groundwater Monitoring and Remediation*, *40*(3), 75–88. https://doi.org/10.1111/GWMR.12398

Lekmine, G., Bastow, T. P., Johnston, C. D., & Davis, G. B. (2014). Dissolution of multi-component LNAPL gasolines: The effects of weathering and composition. *Journal of Contaminant Hydrology*, *160*, 1–11. https://doi.org/10.1016/j.jconhyd.2014.02.003

Lenhard, R. J., Oostrom, M., & Dane, J. H. (2004). A constitutive model for air–NAPL–water flow in the vadose zone accounting for immobile, non-occluded (residual) NAPL in strongly water-wet porous media. *Journal of Contaminant Hydrology*, *73*(1–4), 283–304. https://doi.org/10.1016/J.JCONHYD.2004.07.005

Lenhard, R. J., Sookhak Lari, K., Rayner, J. L., & Davis, G. B. (2018). Evaluating an analytical model to predict subsurface LNAPL distributions and transmissivity from current and historic fluid levels in groundwater wells: Comparing results to numerical simulations. *Groundwater Monitoring & Remediation*, *38*(1), 75–84. https://doi.org/10.1111/GWMR.12254

Li, P., Karunanidhi, D., Subramani, T., & Srinivasamoorthy, K. (2021). Sources and consequences of groundwater contamination. *Archives of Environmental Contamination and Toxicology*, *80*(1), 1–10. https://doi.org/10.1007/S00244-020-00805-Z/FIGURES/2

Libera, A., de Barros, F. P. J., Faybishenko, B., Eddy-Dilek, C., Denham, M., Lipnikov, K., et al. (2019). Climate change impact on residual contaminants under sustainable remediation. *Journal of Contaminant Hydrology*, *226*, 103518. https://doi.org/10.1016/J.JCONHYD.2019.103518

Lu, G., Clement, T. P., Zheng, C., & Wiedemeier, T. H. (1999). Natural attenuation of BTEX compounds: Model development and field-scale application. *Ground Water*, *37*(5), 707–717. https://doi.org/10.1111/J.1745-6584.1999.TB01163.X

Lueders, T. (2017). The ecology of anaerobic degraders of BTEX hydrocarbons in aquifers. *FEMS Microbiology Ecology*, *93*(1), 220. https://doi.org/10.1093/FEMSEC/FIW220

Mao, B., Liu, Z., Liu, S., Zhang, M., & Lu, T. (2020). Investigation of relative permeability, saturation and capillary pressure relations of NAPL-contaminated sands. *Journal of Soils and Sediments*, *20*(3), 1609–1620. https://doi.org/10.1007/S11368-019-02506-0

Martin, D., Kühl, N., & Satzger, G. (2021). Virtual sensors. *Business & Information Systems Engineering*, *63*(3), 315–323. https://doi.org/10.1007/s12599-021-00689-w

Mastrocicco, M., Colombani, N., & Gargini, A. (2012). Characterization and modeling of a BTEX plume originated by a sulphur rich NAPL source. Retrieved from https://www.researchgate.net/publication/280647793

Maurer, M., & Rittmann, B. E. (2004). Modeling intrinsic bioremediation for interpret observable biogeochemical footprints of BTEX biodegradation: The need for fermentation and abiotic chemical processes. *Biodegradation*, *15*(6), 405–417. https://doi.org/10.1023/b:biod.0000044590.23221.b1

McMahon, P. B., Chapelle, F. H., & Bradley, P. M. (2011). Evolution of redox processes in groundwater. *ACS Symposium Series*, *1071*, 581–597. https://doi.org/10.1021/bk-2011-1071.ch026

Miles, B., Peter, A., & Teutsch, G. (2008). Multicomponent simulations of contrasting redox environments at an LNAPL site. *Ground Water*, *46*(5), 727–742. https://doi.org/10.1111/j.1745-6584.2008.00457.x

Molins, S., Mayer, K. U., Amos, R. T., & Bekins, B. A. (2010). Vadose zone attenuation of organic compounds at a crude oil spill site - interactions between biogeochemical reactions and multicomponent gas transport. *Journal of Contaminant Hydrology*, *112*(1–4), 15–29. https://doi.org/10.1016/j.jconhyd.2009.09.002

Molson, J. W. P., & Eng, I. (2011). BIONAPL/3D: A 3D model for groundwater flow, and multi-component NAPL dissolution with dissolved-phase advective-dispersive transport and biodegradation in porous and fractured porous media user guide. Retrieved from http://sciborg.uwaterloo.ca/~molson/

Morris, B. E. L., Henneberger, R., Huber, H., & Moissl-Eichinger, C. (2013). Microbial syntrophy: Interaction for the common good. *FEMS Microbiology Reviews*, *37*(3), 384–406. https://doi.org/10.1111/1574-6976.12019

Neto, D. C., Chang, H. K., & van Genuchten, M. T. (2016). A mathematical view of water table fluctuations in a shallow aquifer in Brazil. *Ground Water*, *54*(1), 82–91. https://doi.org/10.1111/GWAT.12329

Ng, G. H. C., Bekins, B. A., Cozzarelli, I. M., Baedecker, M. J., Bennett, P. C., & Amos, R. T. (2014). A mass balance approach to investigating geochemical controls on secondary water quality impacts at a crude oil spill site near Bemidji, MN. *Journal of Contaminant Hydrology*, *164*, 1–15. https://doi.org/10.1016/J.JCONHYD.2014.04.006

Ng, G. H. C., Bekins, B. A., Cozzarelli, I. M., Baedecker, M. J., Bennett, P. C., Amos, R. T., & Herkelrath, W. N. (2015). Reactive transport modeling of geochemical controls on secondary water quality impacts at a crude oil spill site near Bemidji, MN. *Water Resources Research*, *51*(6), 4156–4183. https://doi.org/10.1002/2015WR016964

Nordstrom, D., Plummer, L., Wigley, T., Wolery, T., Ball, J., Jenne, E., et al. (1979). A comparison of computerized chemical models for equilibrium calculations in aqueous systems. *ACS Symposium Series*, *1*, 857–892. https://doi.org/10.1021/bk-1979-0093.ch038

Ololade, I. A., Arogunrerin, I. A., Oladoja, N. A., Ololade, O. O., & Alabi, A. B. (2021). Concentrations and toxic equivalency of polycyclic aromatic hydrocarbons (PAHs) and polychlorinated biphenyl (PCB) congeners in groundwater around waste dumpsites in south-west Nigeria. *Archives of Environmental Contamination and Toxicology*, *80*(1), 134–143. https://doi.org/10.1007/S00244-020-00790-3

Pandolfo, E., Caracciolo, A. B., & Rolando, L. (2023). Recent advances in bacterial degradation of hydrocarbons. *Water*, *15*(2), 375. https://doi.org/10.3390/w15020375

Park, E., & Parker, J. C. (2008). A simple model for water table fluctuations in response to precipitation. *Journal of Hydrology*, *356*(3–4), 344–349. https://doi.org/10.1016/J.JHYDROL.2008.04.022

Parkhurst, D. L., & Appelo, C. A. J. (2000). User's guide to PHREEQC (version 2)--A computer program for speciation, batch-reaction, one-dimensional transport, and inverse geochemical calculations. Retrieved from https://wwwbrr.cr.usgs.gov/projects/GWC_coupled/phreeqc/html/final.html

Peter, O. (2010). Biological remediation of hydrocarbon and heavy metals contaminated soil. Retrieved from www.intechopen.com

Picone, S. (2012). Transport and biodegradation of volatile organic compounds: Influence on vapor intrusion into buildings.

Pishgar, R., Hettiaratchi, J. P., & Chu, A. (2022). Natural source zone depletion (NSZD) quantification techniques: Innovations and future directions. *Sustainability*, *14*(12), 7027. https://doi.org/10.3390/SU14127027

Pollock, D. W., (2017). Modpath v7.2.01: A particle-tracking model for MODFLOW: U.S. *Geological Survey Software Release*, https://doi.org/10.5066/F70P0X5X

Prommer, H., Anneser, B., Rolle, M., Einsiedl, F., & Griebler, C. (2009). Biogeochemical and isotopic gradients in a BTEX/PAH contaminant plume: Model-based interpretation of a high-resolution field data set. *Environmental Science and Technology*, *43*(21), 8206–8212. https://doi.org/10.1021/es901142a

Prommer, H., Barry, D. A., & Davis, G. B. (2002). Modelling of physical and reactive processes during biodegradation of a hydrocarbon plume under transient groundwater flow conditions. Retrieved from www.elsevier.com/locate/jconhyd

Prommer, H., & Post, V. (2010). A reactive multicomponent transport model for saturated porous media. Retrieved from http://www.pht3d.org

Rama, F., Ramos, D. T., Müller, J. B., Corseuil, H. X., & Miotliński, K. (2019). Flow field dynamics and high ethanol content in gasohol blends enhance BTEX migration and biodegradation in groundwater. *Journal of Contaminant Hydrology*, *222*, 17–30. https://doi.org/10.1016/j.jconhyd.2019.01.003

Robinson, C., Brovelli, A., Barry, D. A., & Li, L. (2009). Tidal influence on BTEX biodegradation in sandy coastal aquifers. *Advances in Water Resources*, *32*(1), 16–28. https://doi.org/10.1016/J.ADVWATRES.2008.09.008

Ross, J. (2013). Groundwater monitoring program newcastle gas storage facility project i groundwater monitoring program newcastle gas storage facility document revision history F nicola fry for HWC and NOW 6 monthly AGL-HWC-NOW meeting.

Rotzoll, K., & El-Kadi, A. I. (2008). Estimating hydraulic properties of coastal aquifers using wave setup. *Journal of Hydrology*, *353*(1–2), 201–213. https://doi.org/10.1016/j.jhydrol.2008.02.005

Rusydi, A. F., Onodera, S. I., Saito, M., Ioka, S., Maria, R., Ridwansyah, I., & Delinom, R. M. (2021). Vulnerability of groundwater to iron and manganese contamination in the coastal alluvial plain of a developing Indonesian city. *SN Applied Sciences*, *3*(4), 1–12. https://doi.org/10.1007/S42452-021-04385-Y/FIGURES/7

Salanitro, J. P. (1993). The role of bioattenuation in the management of aromatic hydrocarbon plumes in aquifers. *Groundwater Monitoring & Remediation*, *13*(4), 150–161. https://doi.org/10.1111/J.1745-6592.1993.TB00459.X

Schmidt, F., Wainwright, H. M., Faybishenko, B., Denham, M., & Eddy-Dilek, C. (2018). In situ monitoring of groundwater contamination using the kalman filter. *Environmental Science and Technology*, *52*(13), 7418–7425. https://doi.org/10.1021/ACS.EST.8B00017

Schreiber, M. E., & Bahr, J. M. (2002). Nitrate-enhanced bioremediation of BTEX-contaminated groundwater: Parameter estimation from natural-gradient tracer experiments. *Journal of Contaminant Hydrology*, *55*(1–2), 29–56. https://doi.org/10.1016/s0169-7722(01)00184-x

Schreiber, M. E., Carey, G. R., Feinstein, D. T., & Bahr, J. M. (2004). Mechanisms of electron acceptor utilization: Implications for simulating anaerobic biodegradation. *Journal of Contaminant Hydrology*, *73*(1–4), 99–127. https://doi.org/10.1016/j.jconhyd.2004.01.004

Sheskin, D. J. (2020). Handbook of parametric and nonparametric statistical procedures. In *Handbook of parametric and nonparametric statistical procedures* (5th ed.). https://doi.org/10.1201/9780429186196

Spence, M. J., Bottrell, S. H., Thornton, S. F., Richnow, H. H., & Spence, K. H. (2005). Hydrochemical and isotopic effects associated with petroleum fuel biodegradation pathways in a chalk aquifer. *Journal of Contaminant Hydrology*, *79*(1–2), 67–88. https://doi.org/10.1016/j.jconhyd.2005.06.003

Suarez, M. P., & Rifai, H. S. (2004). Modeling natural attenuation of total BTEX and benzene plumes with different kinetics. *Groundwater Monitoring & Remediation*, *24*(3), 53–68. https://doi.org/10.1111/J.1745-6592.2004.TB01292.X

Teramoto, E. H., & Chang, H. K. (2019). Geochemical conceptual model of BTEX biodegradation in an iron-rich aquifer. *Applied Geochemistry*, *100*, 293–304. https://doi.org/10.1016/j.apgeochem.2018.11.019

Teramoto, E. H., Vogt, C., Martins Baessa, M. P., Polese, L., Soriano, A. U., Chang, H. K., & Richnow, H. H. (2020). Dynamics of hydrocarbon mineralization characterized by isotopic analysis at a jet-fuel-contaminated site in subtropical climate. *Journal of Contaminant Hydrology*, *234*, 103684. https://doi.org/10.1016/j.jconhyd.2020.103684

Thorn, K. A., & Aiken, G. R. (1998). Biodegradation of crude oil into nonvolatile organic acids in a contaminated aquifer near Bemidji, Minnesota. *Organic Geochemistry*, *29*(4), 909–931. https://doi.org/10.1016/S0146-6380(98)00167-3

Thouement, H. A. A., & Van Breukelen, B. M. (2020). Virtual experiments to assess opportunities and pitfalls of CSIA in physical-chemical heterogeneous aquifers. https://doi.org/10.1016/j.jconhyd.2020.103638

Todd, D. K. (1980). *Groundwater hydrology* (2nd ed.). John Wiley and Sons.

Uçankuş, T., & Ünlü, K. (2008). The effect of aquifer heterogeneity on natural attenuation rate of BTEX. *Environmental Geology*, *54*(4), 759–776. https://doi.org/10.1007/s00254-007-0861-0

Union, E. (2020). Directive (EU) 2020/2184 of the European Parliament and of the Council of 16 December 2020 on the quality of water intended for human consumption.

US EPA. (2003). A review of emerging sensor technologies for facilitating long-term ground water monitoring of volatile organic compounds.

Valsala, R., & Govindarajan, S. K. (2018). Interaction of dissolution, sorption and biodegradation on transport of BTEX in a saturated groundwater system: Numerical modeling and spatial moment analysis. *Journal of Earth System Science*, *127*(4), 53. https://doi.org/10.1007/s12040-018-0950-3

Van Breukelen, B. M., Griffioen, J., Röling, W. F. M., & Van Verseveld, H. W. (2004). Reactive transport modelling of biogeochemical processes and carbon isotope geochemistry inside a landfill leachate plume. *Journal of Contaminant Hydrology*, *70*(3–4), 249–269. https://doi.org/10.1016/J.JCONHYD.2003.09.003

Vencelides, Z., Sracek, O., & Prommer, H. (2007). Modelling of iron cycling and its impact on the electron balance at a petroleum hydrocarbon contaminated site in Hnevice, Czech Republic. *Journal of Contaminant Hydrology*, *89*(3–4), 270–294. https://doi.org/10.1016/j.jconhyd.2006.09.003

Virtanen, P., Gommers, R., Oliphant, T. E., Haberland, M., Reddy, T., Cournapeau, D., et al. (2020). SciPy 1.0: Fundamental algorithms for scientific computing in Python. *Nature Methods*, *17*(3), 261–272. https://doi.org/10.1038/s41592-019-0686-2

Vitens (2021). Vitens/phreeqpython: Object-oriented python wrapper for the VIPhreeqc module (Version 2.0). [Software]. *GitHub*. https://github.com/Vitens/phreeqpython/tree/master

Worrall, F., Swank, W. T., & Burt, T. P. (2003). Changes in stream nitrate concentrations due to land management practices, ecological succession, and climate: Developing a systems approach to integrated catchment response. *Water Resources Research*, *39*(7), 1177. https://doi.org/10.1029/2000WR000130,7

Wu, C. L. R. (2024). Virtual experiments with reactive transport modelling using FloPy: Transport and degradation of dissolved petroleum hydrocarbons in groundwater. [Database]. *4TU.ResearchData*. https://doi.org/10.4121/f7742f02-ee3a-4a84-adf1-625b4a9fd703

Wu, P., Comte, J. C., Zhang, L., Wang, S., & Chang, B. (2021). Effect of surface water level fluctuations on the performance of near-bank managed aquifer recharge from injection wells. *Water*, *13*(21), 3013. https://doi.org/10.3390/W13213013

Wu, Q., Zhang, X., & Zhang, Q. (2017). Current situation and control measures of groundwater pollution in gas station. *IOP Conference Series: Earth and Environmental Science*, *94*(1), 012005. https://doi.org/10.1088/1755-1315/94/1/012005

Xu, Z., Chai, J., Wu, Y., & Qin, R. (2015). Transport and biodegradation modeling of gasoline spills in soil–aquifer system. *Environmental Earth Sciences*, *74*(4), 2871–2882. https://doi.org/10.1007/s12665-015-4311-0

Xu, Z., Serata, R., Wainwright, H., Denham, M., Molins, S., Gonzalez-Raymat, H., et al. (2022). Reactive transport modeling for supporting climate resilience at groundwater contamination sites. *Hydrology and Earth System Sciences*, *26*(3), 755–773. https://doi.org/10.5194/HESS-26-755-2022

Zammouri, M., & Ribeiro, L. (2017). Analyzing the effect of transmissivity uncertainty on the reliability of a model of the northwestern Sahara aquifer system. *Journal of African Earth Sciences*, *129*, 910–922. https://doi.org/10.1016/J.JAFREARSCI.2017.02.034

Zanello, V., Scherger, L. E., & Lexow, C. (2021). Assessment of groundwater contamination risk by BTEX from residual fuel soil phase. *SN Applied Sciences*, *3*(3), 1–20. https://doi.org/10.1007/S42452-021-04325-W/TABLES/5

Zheng, C., Hill, M. C., Cao, G., & Ma, R. (2012). MT3DMS: Model use, calibration, and validation. *Transactions of the ASABE*, *55*(4), 1549–1559. https://doi.org/10.13031/2013.42263

Ziegler, B. A., Schreiber, M. E., & Cozzarelli, I. M. (2017). The role of alluvial aquifer sediments in attenuating a dissolved arsenic plume. *Journal of Contaminant Hydrology*, *204*, 90–101. https://doi.org/10.1016/J.JCONHYD.2017.04.009

Lohman, S. W. (1972). *Groundwater Hydraulics*, 708. U.S Geological Survey Professional Paper. https://doi.org/10.3133/pp708